ELECTROCHEMICAL PROPERTIES OF FLEXIBLE ELECTRODES FOR IMPLANTED NEUROMUSCULAR EXCITATION APPLICATIONS

ELECTROCHEMICAL PROPERTIES OF FLEXIBLE ELECTRODES FOR IMPLANTED NEUROMUSCULAR EXCITATION APPLICATIONS

BY

SABA MOHTASHAMI, B.Sc.

A THESIS

SUBMITTED TO THE DEPARTMENT OF ELECTRICAL & COMPUTER ENGINEERING

AND THE SCHOOL OF GRADUATE STUDIES

OF MCMASTER UNIVERSITY

IN PARTIAL FULFILMENT OF THE REQUIREMENTS

FOR THE DEGREE OF

MASTER OF APPLIED SCIENCE

Master of Applied Science (2011) McMaster University

(Electrical & Computer Engineering) Hamilton, Ontario, Canada

TITLE:	ELECTROCHEMICAL PROPERTIES OF FLEXIBLE ELECTRODES FOR IMPLANTED NEUROMUSCULAR EXCITATION APPLICATIONS
AUTHOR:	Saba Mohtashami B.Sc., (Bio-Electrical Engineering) Amirkabir University of Technology (Tehran Polytechnic), Tehran, Iran
SUPERVISOR:	Dr. Matiar R. Howlader, Dr. Thomas E. Doyle
NUMBER OF PAGES:	xv, 93

To my beloved parents

For their openmindedness, unwavering support, patience and unconditional love

Abstract

This thesis investigates the electrochemical performance of flexible implanted electrodes for the purpose of neuromuscular electrical stimulation. Electrodes performance is validated through their conductivity, stability, and charge delivery capacity (CDC) to avoid irreversible faradaic reactions during stimulation. To study these requirements, electrodes were fabricated by depositing platinum (Pt), gold (Au) and titanium (Ti) thin films on the flexible liquid crystal polymer (LCP) substrate. Their electrochemical properties were then studied using surface and interface characterization techniques including atomic force microscopy (AFM), electrochemical impedance spectroscopy (EIS), cyclic voltammetry (CV) and a theoretical model.

The EIS results demonstrate that larger electrodes provide higher conductivity and double layer capacitance. In terms of material, Pt offers the best conductivity in neuromuscular stimulation frequencies of 1- 250 Hz, followed by Ti and Au, respectively. Above 250 Hz, similar values of conductivity is offered by the electrodes. This material dependence of impedance magnitude is related to the surface morphology, structural quality and deposition parameters of the electrodes and is explained using surface roughness measurements and interface model parameters.

Electrode long-term stability is explored by regular EIS measurements through 42-day experiments. With progressing time, an increase in surface roughness, decrease in charge

transfer resistance (R_{ct}) and capacitive quality (β) are observed due to the change in capacitive and faradaic behaviors. However, in the comparative evaluations, Au electrode shows the most consistency in keeping its capacitive behavior to perform reversible charge transfer, followed by Pt and Ti, respectively.

Further, cyclic voltammetry (CV) curves were used to understand the charge transfer reactions and calculate charge delivery capacities (CDC) of Pt, Ti and Au. Pt with highest CDC value suggests the best electrochemical reversibility followed by Au and Ti. In the case of deposition pressure, for Ti electrode, lower deposition pressure yields higher charge delivery capacity.

These results may make lower pressure deposited Pt electrode with high conductivity and CDC the best material for the short term applications of neuromuscular electrical stimulation, while Au possessing improved stability but lower conductivity and CDC is suggested for long term applications. This result provides deeper insight into the design and miniaturization of electrochemical electrodes for the further development of neuromuscular prostheses.

Acknowledgements

I would like to express my sincere gratitude to my supervisors Dr. Matiar R. Howlader and Dr. Thomas E. Doyle for their continuous guidance and support through the course of my M.A.Sc. program at McMaster University. This thesis would not have been possible without their invaluable suggestions and encouragement.

Many thanks and appreciation to Fangfang Zhang for her work in the clean room to deposit the electrodes and her kind assistance in surface measurements.

I am specially grateful to Dr. Joey Kish for providing me the access to the Walter W. Smelter Corrosion Laboratory and for his utmost cooperation, invaluable insights and constructive feedbacks.

I would like to extend my appreciation to Mehdi Taheri for his assistance in electrochemical measurements. Without his help, the electrochemical experiments presented in this thesis would have been difficult for me.

I would like to acknowledge my committee members, Dr. Hubert Debruin and Dr. Joey Kish for taking the time to read my thesis, and for providing me with great comments.

Special thanks to my friends and colleagues at McMaster University for making the past two years a wonderful and enjoying time.

I am deeply grateful to M. Hamed Mousazadeh for everything he has done for me during my graduate life in Canada. Thank you Hamed for standing by me from the tough

last moments of leaving my family at the airport through this roller coaster ride. Thanks for encouraging me to work harder toward our common target. Thanks for teaching me how to "give and forgive" and showing me how to love unconditionally but with patience. For picking me up whenever I fall and still having faith in me all the way through. Thank you for being the big inspiration of my life, and for bringing cheer to my life by being there for me all over the journey we have started together.

Finally, I owe my deepest gratitude to my beloved grandmother, mother, father and sister, whose open-mindedness, unwavering support, patience, and unconditional love made me who I am today.

Notation and abbreviations

AFM : Atomic Force Microscopy

Au : Gold

CDC : Charge Delivery Capacity

C_{dl} : Double Layer Capacitance

CPE : Constant Phase Element

CV : Cyclic Voltammetry

EIS : Electrochemical Impedance Spectroscopy

f_c: Cut-off Frequency

FES : Functional Electrical Stimulation

Ir : Iridium

IrO_2 : Iridium Oxide

LCP : Liquid Crystal Polymer

NMES : Neuromuscular Electrical Stimulation

PBS : Phosphate Buffered Saline

Pt : Platinum

R_{ct} : Charge Transfer Resistance

R_e: Electrolyte Resistance

RMS : Root Mean Square

SCE : Saturated Calomel Electrode

Si : Silicon

Ti : Titanium

Contents

List of Figures

Chapter 1

Introduction

1.1 Motivation

There are many muscle control disorders due to the absence or failure of neural impulses reaching their natural destination. In these cases, while peripheral nerves and muscles are still intact, the patient does not have the ability to activate them voluntarily. Intact nerves can be activated via the electrodes by external signals through electrical stimulation [7]. Therefore, electrical stimulation has been widely utilized by many research groups [8–12].

The electrical stimulation techniques require a means of generating an electric pulse, a way to route the pulse to the nerve, and electrodes to deliver an effective stimulus to the nerve to activate the target tissue. These techniques share common design constraints of the requirements of lower power consumption, small size, and the capability of effective and safe stimulation [12, 13]. To accomplish effective and safe stimulation, the designer must balance the amount of stimulus current (high) against the device size and power (increased with higher current). An area to optimize these requirements is the stimulating electrode. Stimulating electrodes, if understood, fabricated and characterized precisely, could offer

more efficient electrical stimulation, with low power consumption and minimal, if any, electrode-tissue interface injuries.

Compared to other methods of electrical stimulation such as transcutaneous and percutaneous stimulation, implanted electrodes provide better selectivity, lower stimulation current intensity, and reduced rate of fatigue [14]. However, there exist some challenges due to the invasiveness of implanted electrodes. For instance, inserting an external object in the body causes electrochemical and mechanical issues that limit the application of implanted electrodes. Neuromuscular stimulation electrodes face electrochemically harsh working conditions. These electrodes, in contact with body tissue, must be non toxic and non reactive with the surrounding environment. That means while injecting a high amount of charge, they should avoid the formation of any dangerous reactions. Electrodes should also function without facing corrosion during the device lifetime.

In addition to electrochemical considerations, mechanical fitness is another issue in electrodes design. Providing good fitness, electrodes should not cause any compression or damage to the tissue. The above challenges and many more underscore the importance of research in design and characterization of implantable electrodes. Study in this area is required to address some of the key issues currently inhibiting widespread adoption of implanted stimulation technologies.

1.2 Problem Statement and Thesis Contribution

To overcome the mechanical obstacles such as abrasive or compressive injuries and fitness difficulties in the application of electrodes with rigid substrates, flexible substrates have emerged [1–3]. Flexible substrates provide a safer excitation by moving with the nerves which applies no compression on them. They also enhance mechanical fixation

which increases the charge transfer at electrode/tissue interface. Preference of flexibility leads the electrode material technology toward using biocompatible polymers as electrode substrates.

Most of the current implanted electrodes are designed on Polyimide (PI) substrate. PI is a common flexible substrate in electrical stimulation electrodes [1–3, 15, 16]. However, it suffers from high water absorption [17]. Water absorption causes hydrolytic attack of the substrate material that results in delamination of deposited electrodes at adhesion layer/polyimide interface.

To overcome this challenge, we present liquid crystal polymer (LCP) as the flexible substrate material in this study. To the best of our knowledge, there is no comparative evaluation of LCP substrates in neuromuscular stimulation electrodes. Compared to other flexible substrates, such as PI, LCP has a little water absorption [17], which provides better electrochemical stability of electrodes for long term applications.

Further, implanted electrodes should be electrochemically appropriate for the purpose of neuromuscular stimulation. They should offer relatively low impedance in transferring electrical impulses from the electrodes to ions in the surrounding electrolyte. Low impedance provides excitation at a lower amount of injected charge. They also require to provide charge delivery capability that avoids the harmful chemical changes in both tissue fluid and electrodes, that may destroy electrodes and produce undesirable toxic products.

The factors that control these electrochemical properties include electrodes material, their size and deposition parameters (such as deposition technique, deposition pressure, etc). Therefore, to investigate the electrochemical properties of stimulation electrodes on LCP each factor is comparatively studied. Three biocompatible metals are selected as the

conducting layers. Platinum (Pt), gold (Au), and titanium (Ti) films were deposited at different sizes on LCP. Another set of Ti specimens was deposited at a different deposition pressure. Ti was selected for studying the effect of deposition pressure as it is more prone to show different behavior with changing deposition conditions. The reason is that Ti is more reactive compared to Pt and Au. Hence, possible contaminations that are due to poor vacuuming of higher deposition pressure, possibly form a thin passive oxide layer on the top of the deposited film [18,19]. Therefore, Ti electrochemical performance is more likely to be influenced by changing the deposition pressure. The target was to evaluate electrode charge transfer parameters and longevity at the presence of LCP as their substrate. Electrodes were fabricated in four circular surface areas to evaluate the effect of electrode size on electrode-tissue impedance. Electrochemical investigation of deposited films in the biological environment was performed by electrochemical impedance spectroscopy (EIS) and cyclic voltammetry (CV). The EIS and CV measurements were performed at room temperature in 0.1-molar phosphate buffered saline (PBS) solution. PBS is a saline solution containing sodium chloride, sodium phosphate, potassium phosphate and potassium chloride, and is commonly used as the physiological medium in biological research [1–3, 20]. Root mean square (RMS) surface roughness, impedance magnitude spectra, and the equivalent circuit model of the electrode/electrolyte interface of the three electrode types were studied to evaluate the electrodes charge transfer parameters and to research their usefulness in different neuromuscular prosthetic applications.

It should be noted that the temperature and speed of the performed experiments are selected from an electrochemical perspective but are different from those of real physiological applications. However, these values are selected to be as close to the real application values as the available equipment allow.

1.3 Organization of the thesis

The rest of this thesis is organized as follows:

In chapter 2, the basic physiology of peripheral nerves activation followed by the targeted neurological disorders is presented. Then electrical stimulation system and its components are introduced. Stimulation electrodes due to their significance in neuromuscular activation have been the subject of extensive research and therefore, are focused in this review. Finally, different approaches addressing the challenges concerning the electrodes that are applicable to neuroprosthetic devices are reviewed. The addressed challenges include biocompatibility, mechanical considerations and charge transfer parameters.

Chapter 3 focuses on the basic principles and relevant experimental aspects of the surface and interface characterization techniques. An equivalent circuit model is presented for evaluating the electrodes charge transfer parameters and to research their physical functionalities in neuromuscular prosthetic applications.

In Chapter 4, the electrochemical interfacial impedance is discussed for different electrode sizes, materials, and deposition pressures. Chapter 4 also presents the longevity evaluations of different electrode materials using the interface model and electrochemical impedance spectra.

Chapter 5 discusses charge transfer mechanisms of different electrodes using cyclic voltammetry technique. The charge delivery capacity values and their dependence on deposition pressure are presented in comparison with literature.

Chapter 6 provides a full perspective discussion of the thesis. This discussion includes all the results proposed in chapter 4 and 5.

The thesis is concluded in Chapter 7 where some possible directions for future research are also suggested.

1.4 Scope

The purview of this study encompasses electrochemical investigation of implanted electrodes for the purpose of electrical stimulation. It presents fabrication of biocompatible electrodes using Pt, Au and Ti as conducting layers and flexible LCP as the substrate material. Deposited electrodes are then investigated through surface and interface characterization techniques. Surface characterization is performed by assessing RMS surface roughness using atomic force microscope. Interface characterization includes electrochemical impedance spectroscopy (EIS) and cyclic voltammetry (CV). EIS data is fitted to an equivalent circuit model to provide electrochemical parameters of immersed electrodes in the electrolyte. Explaining the functionalities, these derived parameters evaluate the electrodes performance. CV data is used to study charge transfer mechanisms of electrodes under conditions similar to those of stimulation. The results of these evaluations are verified with surface characterization experimental data. Improved electrodes are introduced based on their lower electrode/electrolyte impedance, better longevity and higher charge delivery capacity.

1.5 Related Publications

- S. Mohtashami, M. R. Howlader, T. E. Doyle, and J. Kish,"Charge Transfer and Stability of Implantable Electrodes on Flexible Substrate for Neuromuscular Excitation", Applied Physics Letters, Submitted.

- S. Mohtashami, M. R. Howlader, and T. E. Doyle, "Comparative Electrochemical Investigation of Pt, Au and Ti Electrodes on Liquid Crystal Polymer for the Application of Neuromuscular Prostheses", ECS Transaction, Accepted.

- S. Mohtashami, M. R. Howlader, T. Doyle, and M. Taheri,"Comparative Electrochemical Investigation of Pt, Au and Ti Electrodes on Liquid Crystal Polymer for the Application of Neural Prostheses", 219th ECS Conference, May 1-6, Montreal, Canada (2011).

Chapter 2

Electrodes in Electrical Stimulation Systems

This chapter presents a brief review of the previous studies in electrical stimulation systems focusing on stimulation electrodes and their parameters. First, a general overview of the physiology of peripheral nerves activation followed by the targeted neurological disorders is presented. Then electrical stimulation system and its components are introduced. Stimulation electrodes due to their significance in neuromuscular activation have been subject of extensive research and therefore, are focused in this review. Finally, different approaches addressing the challenges concerning the electrodes that are applicable to neuromuscular prosthetic devices are reviewed.

2.1 Physiological Overview

Peripheral nerves control muscle movement by transmitting impulses from the spinal cord to muscle fibers. Many neurological disorders are caused by the absence or failure of neural impulses to reach their natural destination. For instance, for the case of stroke and spinal cord injuries, while peripheral nerves and muscles are still intact, the patient doesn't have the ability to activate them voluntarily [7]. In this case, intact peripheral nerves could activate muscle fibers if stimulated artificially. In general, through stimulation, an impulse is applied to muscle or nerve directly, or to a motor point adjacent to neuromuscular junction. This impulse, similar to action potential, results in the activation of the nerves that control muscle contraction [21]. Motor point is the most electrically excitable area of the muscle that exhibits the most robust contraction at the lowest level of stimulation [22], and is usually located at the center of the muscle mass where the motor nerve enters muscle. Figure 2.1 is a schematic diagram showing the transmission of action potential by peripheral nerves toward muscle fibers. The action potential induced by neuromuscular electrical stimulation (NMES) is propagated similarly to the natural physiological action potential along the axon from the cell body toward the distal portion of the axon. Its pathway along the axon is similar to a single active wire towards the intact muscle fibers. Thereby, the muscle fibers are contracted resulting in function for a nonfunctional limb or tissue with intact nerves.

However there is a difference in fiber activation between NMES activated and naturally activated muscle fibers. There are two main classes of muscle fibers:

- Fast-twitch muscle fibers
- Slow-twitch muscle fibers

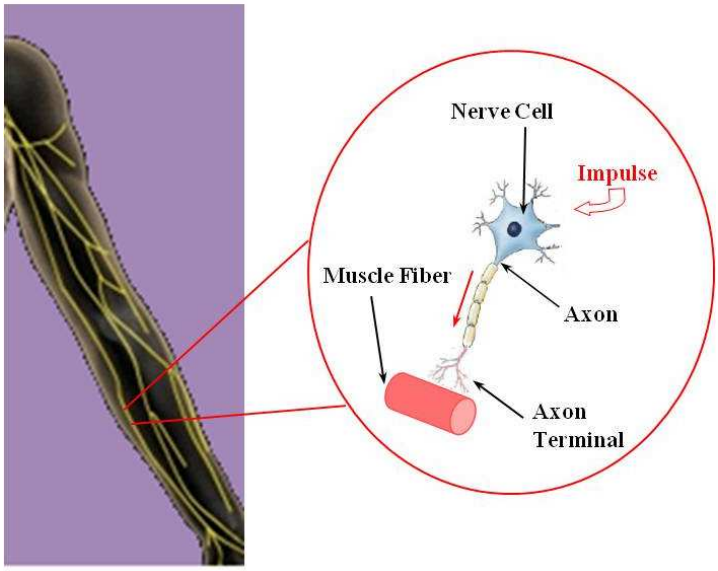

Figure 2.1: Schematic diagram showing the transmission of action potential by peripheral nerves toward muscle fibers. Neurons (nerve cells) receive information from the impulse and pass that through their axons by propagation of the action potential down the axon toward the muscle fiber.

Larger nerves innervate fast-twitch muscle fibers. Fast-twitch muscle fibers generate higher forces but fatigue so quickly. Slow-twitch muscle fibers are innervated by smaller nerves and are more fatigue resistant. Natural mechanism recruits smaller nerves prior to larger ones. However, NMES reversely activates the larger nerve fibers prior to smaller ones which happens due to the lower excitation thresholds of larger fibers in external stimulation. Therefore, chronic use of NMES causing reverse recruitment, results in rapid muscle fatigue. To counter fatigue challenge, a selective stimulation system is required that enables the prior stimulation of fatigue resistant smaller fibers.

2.2 Electrical Stimulation Systems

Adequate stimulus to provide functionality in muscle may be chemical, mechanical, thermal or electrical. However, there is a major challenge in chemical, mechanical and thermal stimulations. Compared to electrical stimulation, they require a significantly greater intensity of stimulus to achieve muscle contraction [21]. In fact, electrical stimulation could be conducted with lower power consumption. Therefore, electrical stimulation has been widely utilized by many research groups as the basis of emerging prostheses and treatments for spinal cord injuries, stroke, sensory deficits and neurological disorders [8], for control of respiration, bowel and bladder, restoring vision sense at outer retina and providing partial hearing [9–12].

The electrical stimulation techniques require a means of generating an electric pulse, a way to route the pulse to the muscle, and electrodes to deliver an effective stimulus to the nerve to activate the target muscle. There are some common design challenges in these techniques including the need of lower power consumption, small size, and the capability of effective and safe stimulation [12, 13]. To accomplish the last requirement, if the stimulus current is high, the device size and power may increase. An area to optimize these requirements is the stimulating electrode. Hence, stimulating electrodes are of great importance in achieving more efficient electrical stimulation, with low power consumption and no or only minimal electrode-tissue interface injuries, and thus different types of them should be understood precisely.

Based on the current electrical stimulation systems, stimulating electrodes fall into two broad categories:

1. Surface electrodes

Figure 2.2: A pair of TENS Electrode, product of *Protens* to provide the conductive interface between the TENS generator and the patients skin.

2. Implanted electrodes

Surface electrodes are utilized in transcutaneous electrical stimulation (TES). TES provides non-invasive activation of excitable tissue in the human body using electrical current produced by a device injected through surface electrodes. This technique is also applied to reduce pain; both acute and chronic in trancutaneous electrical nerve stimulation (TENS), in rehabilitation of stroke subjects or spinal cord injuries (SCI) as functional electrical stimulation (FES), or as neuroprostheses for supporting tasks in daily living [21,23]. Figure 2.2 shows a pair of surface electrodes for TENS applications.

Although TES is a non-invasive technique, there exists a number of obstacles. Some reported obstacles include (a) cutaneous discomfort for patients, (b) difficulties in providing a good electrode-skin contact, (c) unwanted activation in overlying superficial muscles while targeting to stimulate deeper muscles, (d) high rate of muscle fatigue, (e) required clinical skills to place electrodes and adjust stimulation parameters [21,24]. These obstacles make TES difficult to be optimal, tolerable and consistent. To overcome these challenges and to

get more efficient activations, studies have been shifted toward implanted electrical stimulation systems. In order to deliver an effective stimulus to the nerve to activate the target tissue, implanted stimulation devices need to utilize implantable electrodes.

2.3 Implanted Stimulation Electrodes

Implantable electrodes are used in implanted electrical stimulation systems. Based on the target of the treatment or recovery process, several implanted electrical stimulation techniques are designed that utilize different kinds of electrodes. Implanted peripheral neuromuscular electrical stimulation electrodes are categorized according to their position relative to the muscle or nerve trunk. They could be either percutaneous intramuscular, epimysial, intraneural or nerve cuff systems. The last three require open surgical procedures to be implanted [21]. While they do not cause cutaneous discomfort, better selectivity is achieved by elimination of skin resistance [21]. In addition, since stimulation is directly applied to the nerves or a motor point adjacent to neuromuscular junction, lower stimulation intensity is required to provoke the excitation. However, there still exist some challenges due to the invasiveness of these techniques. For instance, inserting external object in body brings electrochemical and mechanical issues of concern. These issues include biocompatibility, mechanical fitness and charge transfer mechanisms.

2.3.1 Biocompatibility

The primary challenge of designing an implanted electrode has always been its biocompatibility in contact with host tissue [2,25,26]. A material is considered to be biocompatible if it avoids toxic or immune responses in the adjacent medium and is not degraded by the

organism [7]. For the case of stimulation electrodes, both substrate material and conducting materials need to be biocompatible. Several types of neuromuscular electrodes have been designed that use silicon [27–29], ceramic materials [30] and flexible substrates [31–33] as the electrodes substrate material, all of which are biocompatible. Electrode conducting materials such as platinum (Pt), gold (Au), titanium (Ti), iridium (Ir), and iridium oxide (IrO_2) have been studied which are well tolerated by the tissue with no toxicity concern; [3, 15, 26] however, for Ir and IrO_2 stimulation electrodes on PI substrate, in vivo delamination is reported [8]. The biocompatibility of four different electroactive polymers has been investigated [34]. After the subcutaneous implantations, the specimens were in the animals bodies (beneath the dorsal skin) for the ranges of 19 to 90 weeks, during which some physical and histological examinations were done. They studied behavioral differences, any lesions or infections on the skin surface. Their research substantiates that these polymers are biocompatible and highly demanded for biomedical applications [34, 35]. Other emerging biocompatible materials utilized in neuromuscular electrodes are nanotube materials, such as carbon nanotubes (CNT) [36, 37] as well as conductive polymer nanotubes [38].

2.3.2 Mechanical Concerns

Beyond biocompatibility, electrodes should be mechanically safe. There are many mechanical obstacles in the application of electrodes with rigid substrates including thickened epineurium (the outmost layer surrounding the peripheral nerve) due to accumulation of connective tissue beneath the electrode, and abrasive injury in the form of subperineural crescents on the outer side of fascicles [39]. In order to prevent such damage, electrodes should follow some principles: the electrode should fit the nerve with no compression, so

that electrode moves with the nerve, which minimizes abrasion from relative movement of the nerve and electrode. In addition, practically there is a physical gap between conducting material and the body tissue. This gap determines the current and charge thresholds required for cell activation in stimulating applications, and hence is an issue of concern. Therefore, precise formation of electrode is required to minimize this critical gap. Further, in most implanted stimulation techniques, after implantation is performed, tissue swelling occurs. Soft and flexible electrodes are preferred as they are easier to fit the body tissue and allow self-sizing in the case of edema after implantation. Flexible substrate materials are of great interest if they are biocompatible. Flexibility helps avoid passive mechanical damage to the nerve and surrounding tissue. Preference of flexibility leads the electrodes material technology toward using polymers. Recently, polymer substrates have attracted much interest due to their flexibility, biocompatibility, and mechanical strength [1, 15, 25]. Polymer substrates enhance mechanical fixation. In addition, moving with the nerve which applies no compression on it, polymer electrodes minimize abrasion from relative movement of the nerve and electrode, and finally, providing a better electrode- tissue contact, they increase the charge transfer at electrode/tissue interface. Polyimide (PI) is an insulating biocompatible material with various applications in biomedical devices. Due to its advantages of thermal stability, good chemical resistance and excellent mechanical properties, PI is commonly used as a flexible substrate in electrical stimulation electrodes [1–3, 16, 17, 31, 33].

F. J. Rodriguez *et. al* [16] fabricated a spiral-cuff electrode of polyimide for stimulating peripheral nerves. As shown in Figure 2.3, three integrated circumneural platinum electrodes were attached to an external biocompatible plastic connector by a thin polyimide ribbon. Their *in vivo* study reported no harm to the host. Polyimide cuff electrodes were reported to be mechanically harmless while enhancing the stimulation of peripheral nerves

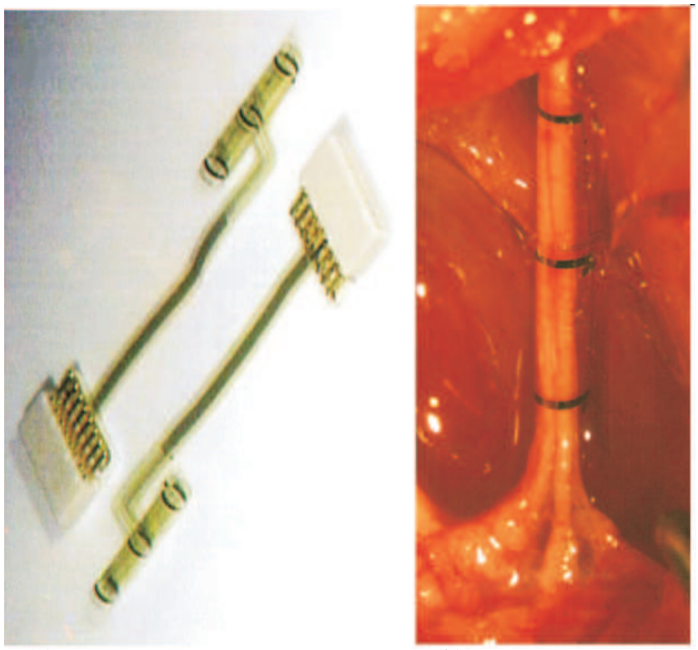

(a) (b)

Figure 2.3: Polyimide cuff electrode used in Rodriguez *et. al* study; (a) Cuff electrode and connector, and (b) its implantation around the sciatic nerve of a rat before performing the experimental study [16].

compared to similar electrodes on rigid substrates. However, PI suffers from high water absorption(3%) [17]. High water absorption causes hydrolytic attack of the substrate material that causes delamination at metal/polyimide interfaces of deposited electrodes. To overcome this challenge, in this study liquid crystal polymer (LCP) is presented as the flexible substrate material. Compared to PI, LCP benefits from the lower water absorption (0.04%). Lower water absorption protects the deposited electrode from delamination of the metal/polymer interface and hence, enhances the electrochemical stability of electrodes for long term applications.

2.3.3 Interfacial Charge Transfer

In addition to biocompatibility and mechanical considerations, stimulation electrodes have to be stable in contact with host tissue. Stability involves efficiently transferring charges by converting free electrons into ions without causing electrode corrosion or electrolyzing the tissue. This charge transfer can occur through three mechanisms:

1. Non-faradaic charge transfer reaction which is the capacitive charging/discharging of double layer at the electrode-electrolyte interface. No electron is transferred between the metal electrode and electrolyte. No chemical changes occur in either the tissue or electrode, so it is the ideal charge transfer reaction.

2. Reversible faradaic charge transfer reactions in which electron transfer between the electrode and the electrolyte is close to the electrode surface. Although the chemical species in the electrolyte undergo reduction or oxidation, a current passed in opposite direction can quantitatively reverse them and no new chemical species is generated in the bulk of the tissue.

3. Irreversible faradaic charge transfer reactions in which the products diffuse away from the electrode. Hence, a current in opposite direction can not reverse them into its initial form. Therefore, they cause harmful chemical changes in both tissue fluid and electrodes and may destroy electrodes and produce toxic products and thus are undesirable.

Enhanced charge transfer is commonly evaluated by employing a reversible charge injection process through either double layer capacitive (non-faradaic) reactions and reversible faradaic charge transfer reactions at electrode/electrolyte interface as shown in

Figure 2.4 [2, 8, 26, 37, 40]. Normally faradaic processes are reported under electrical stimulation because the amount of charge required for metal electrodes to reach the necessary activation greatly exceeds that available from the ideal capacitive transfer only [25, 26]. However, irreversible faradaic charge transfer reactions are avoided. The most common irreversible processes encountered with stimulation electrodes are electrolysis of water, electrode dissolution or corrosion [8]. Therefore, it is important to understand the charge injection mechanism of the electrode to define the reversible charge injection limit. This limit defines the quantity of charge that can be injected or transferred using only reversible processes and is called charge delivery capacity (CDC) [25, 26, 35]. Hence, higher CDC avoids electrodes corrosion or degradation, and harmful changes in the biological environment and makes possible long-term or chronic implantation. In addition, higher value of CDC would require smaller area to transfer certain amount of charge. Since practical applications require miniaturized electrode geometry to control a large number of different muscle fascicles, high charge delivery capacity material is demanded [13, 35]. CDC depends upon electrode size, geometry, deposition conditions and the parameters of stimulation waveform.

In order to investigate the charge transfer parameters, presence of each mechanism and CDC limits, many research groups have performed measurements for electrochemical characterization including electrochemical impedance spectroscopy (EIS) and cyclic voltammetry (CV), as well as surface studies including scanning electron microscopy (SEM) and atomic force microscopy (AFM). N. Tandon *et. al* [2] compared different biocompatible materials including nanoporous carbon, stainless steel, titanium and titanium nitride for cardiac tissue engineering by EIS and SEM measurements, and the equivalent model of electrode/electrolyte interface. Carbon electrodes demonstrated the best charge transfer

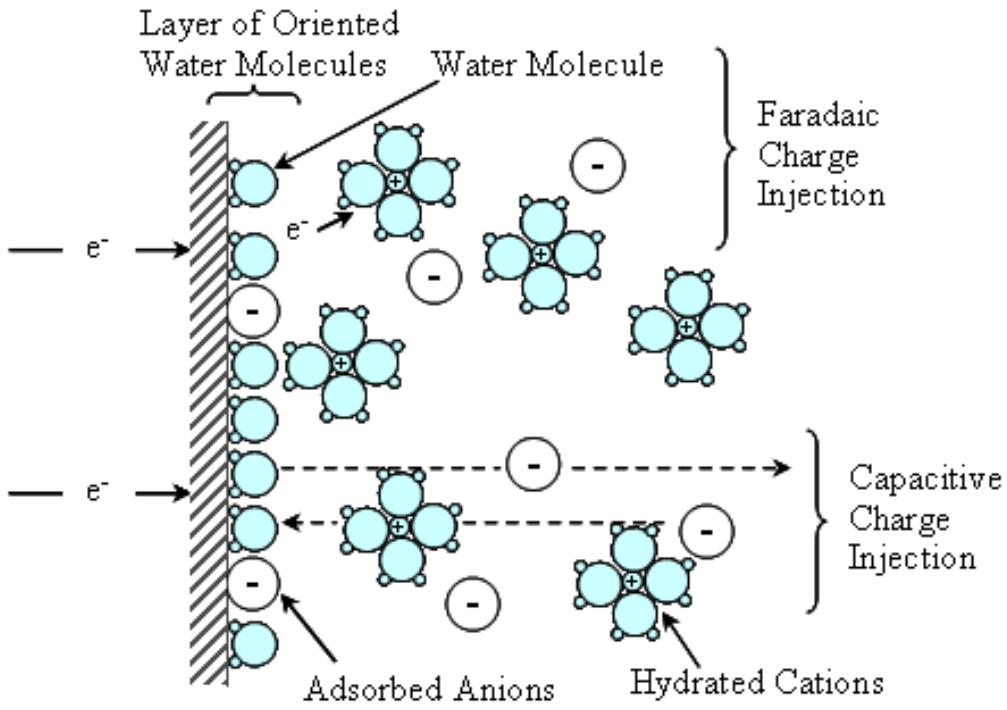

Figure 2.4: Schematic of charge transfer processes at electrode/electrolyte interface showing faradaic charge transfer (*top*) and capacitive charge transfer (*bottom*) as the electrode is driven negative [26] While capacitive charge injection involves redistribution of charge, in faradaic process, electron is transferred from the metal electrode into the electrolyte. This electron transfer could cause reduction or oxidation of chemical species in the electrolyte which may or may not be reversible

parameters. However, their usage is limited due to their poor mechanical strength. Titanium nitride demonstrated improved performance compared to titanium. It offered higher values of electrochemical conductivity and double layer capacitance than those of titanium. Stainless steel showed the most susceptibility to corrosion. J. D. Weiland [13] proposed titanium nitride and iridium oxide bioelectrodes on silicon substrate. Their electrochemical measurements indicated that iridium oxide had lower impedance and a higher charge storage capacity than titanium nitride, suggesting better performance as a stimulating electrode.

S. H. Lee *et. al* [3] developed flexible nerve cuff electrodes with platinum, iridium and iridium oxide films on polyimide substrate by radio frequency (RF) sputtering at different deposition pressures. EIS and CV tests were conducted to investigate the electrochemical properties. Each film deposited at 30 mTorr of working pressure shows the best charge transfer parameters compared to those fabricated at higher or lower pressures. The competing factors include electrodes interfacial impedance magnitude and their charge delivery capacity value. Unlike platinum and iridium, iridium oxide films had symmetrical cyclic voltammograms along the potential axis. This symmetry represents excellent electrochemical reversibility and equal anodic and cathodic charges transferred through the iridium oxide film and the electrolyte interface. It was also found that iridium oxide charge delivery capacity is enhanced by the Ar:O_2 gas flow ratio of 8:1 rather than smaller amounts of oxygen flow. S. Negi *et. al* [20] confirmed the effect of Ar:O_2 gas sputtering pressure on the properties of iridium oxide films. In their study, 5 mTorr was found to be the optimal sputtering pressure compared to other higher sputtering pressures. In 5 mTorr, electrodes offered higher conductivity and charge delivery capacity. They also reported that lower sputtering pressure improved electrical, mechanical and electrochemical characteristics of electrodes by providing denser films which enhanced charge delivery capacity [20]. E.T.

McAdams *et. al* [1] designed gold electrodes in different surface areas and assessed them through EIS and noise measurements. They displayed that smaller electrodes have larger interfacial impedance magnitudes and greater noise. Wang *et. al* [36] developed carbon nanotube microelectrodes with high strength and flexibility. However, they suffer from low charge delivery capacity (CDC) [15].

However, to the best of our knowledge, there is no comparative evaluation of implanted electrodes on LCP substrates for neuromuscular stimulation applications. In order to investigate the electrochemical mechanisms, longevity and CDC limits of electrodes on LCP substrates, this thesis presents a comparative study on Pt, Au, and Ti electrodes on LCP. The evaluations are performed through electrochemical measurements. These measurements address the electrodes' material dependent parameters and their deposition pressures, since they affect the performance of implanted electrodes. Therefore, in this research three electrode materials are selected and deposited in four surface areas and with two base pressures. The measurement results are compared to similar studies in the literature to research the performance of our electrodes of different conditions.

Chapter 3

Experimental Procedure

This chapter focuses on the basic principles and experimental aspects of the electrodes deposition procedure, and surface and interface characterization techniques. The electrodes are fabricated through electron beam evaporation in different sizes and at two different deposition pressures. Their surface is studied using atomic force microscopy. The electrode/electrolyte interface is electrochemically investigated through electrochemical impedance spectroscopy and cyclic voltammetry techniques. A theoretical model of the interface is proposed based on the electrochemical impedance spectra for evaluating the electrodes charge transfer parameters and to research their physical functionalities in neuromuscular prosthetic applications.

3.1 Specimens

In this study, liquid crystal polymer (LCP) was used as the substrate material of electrodes. The LCP was commercially available Vecstar CT X100, 50 μm thick. As for the conducting layer of electrodes, platinum (Pt), gold (Au) and titanium (Ti) were used. Ti also served as the adhesion layer between the LCP substrate and the conducting layer. For the deposition of Pt, Au and Ti films, the purities were 99.99%, 99.999% and 99.99% respectively. To deposit conducting layers on the substrate, a mask was required. To improve the uniformity of electrode's surface, the proposed mask should be from a thin and firm material. Thin mask helps in keeping the similar film thickness all over the deposited electrode's surface specially at the edges. Firmness, making a fit contact, avoids any movement of mask on LCP substrate during evaporation process. Good substrate/mask contact results in more uniform electrodes. Further, the mask should be thermally stable. At high temperature of deposition no deformation should occur. These requirements were accomplished through a 0.1 mm thick copper mask. The mask was prepared by water jetting technique with sharp circular pores of 3, 4, 6, and 8 mm diameters. Figure 3.1 shows a picture of the mask after the deposition. Tails were designed to provide a contact out of the electrodes for the measurements without affecting their surfaces. To improve the reliability of the results, five samples of each size were designed.

After wire connection, tails were covered by insulating glue so that only circular spaces were in effect for charge transfer. Figure 3.2 displays a schematic diagram of a deposited electrode.

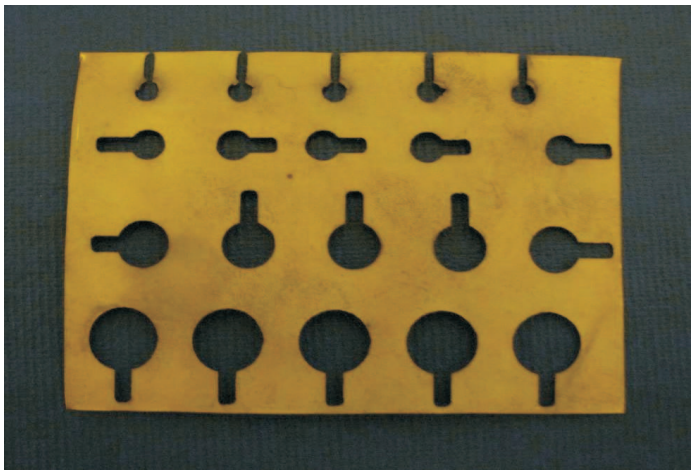

Figure 3.1: 0.1 mm Thick copper mask to be placed on the substrate for electrodes deposition.

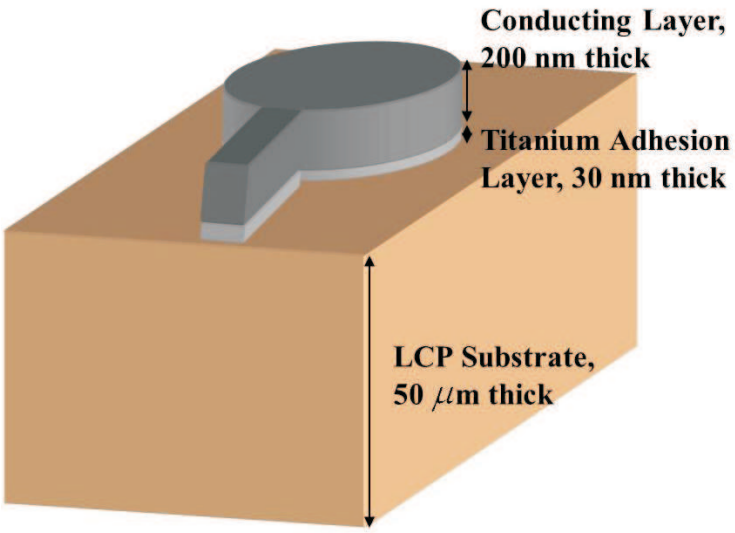

Figure 3.2: A schematic diagram of a deposited electrode on the LCP substrate.

3.2 Deposition Equipment

The electrode fabrication was accomplished using an electron beam evaporation equipment as shown schematically in Figure 3.3. E-beam evaporation is selected as the deposition technique because compared to other techniques such as sputtering, it provides us with more uniform deposited films by rotating the substrate through the evaporation [41]. In addition, it improves the contact of adhesion layer to the LCP substrate. Therefore, e-beam evaporation technique results in better quality of deposited electrodes and thus, is selected. The evaporation system includes vacuum pumps, a loading chamber and a deposition (vacuum) chamber separated by a gate valve. The substrate with the mask on it, was placed inside the loading chamber with topside face down. The door of the loading chamber was closed and the chamber was vacuum pumped. As soon as the vacuum pressure was decreased to 10^{-6} Torr, the gate valve was opened and an mechanical transfer rod was used to transfer the specimens from the loading chamber to the deposition chamber. An ultrahigh vacuum (UHV) pressure was maintained in the deposition chamber. An electron beam was aimed at the source material inside the deposition chamber causing local heating and evaporation. There was a shutter between the e-beam gun and the substrate that opened as evaporation was to begin. Evaporation took place in the vacuum. Vapors other than the source material (such as carbon or oxygen) were almost entirely removed at this vacuum pressure before the process began. However, it should be mentioned that even with ultra high vacuuming, there were still few unwanted molecules remaining in the vacuum that could affect the electrodes surface through their condensation on the top part of deposited film. Although these molecules might be negligible due to their small amount, for some active materials such as Ti, they should be considered while studying the thin films electrical/electrochemical properties. In ultra high vacuum, evaporated particles traveled directly

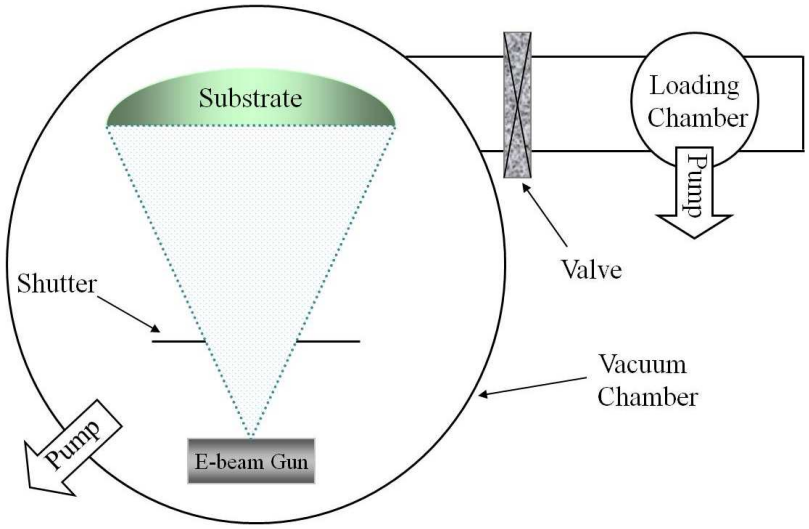

Figure 3.3: Schematic of electron beam evaporation equipment.

to the deposition target and condensed on the substrate surface.

3.3 Electrodes Deposition Procedure

The LCP substrate was first placed in the vacuum chamber. Then, the copper mask was pinned on the LCP substrate firmly. To enhance the adhesion of the conducting layer to LCP substrate, a 30 nm titanium layer was deposited between the conducting layer and LCP. Platinum, gold, and titanium were evaporated as conducting materials with 200 nm thickness. Adhesion and conducting layers were deposited through electron beam evaporation technique at deposition rate of 1.5 $\frac{\mathring{A}}{s}$ with background pressure of 10^{-6} Torr. To investigate the effect of deposition pressure on electrodes performance, another set of titanium samples was deposited using the same technique and parameters at background pressure of 3×10^{-8} Torr. Figure 3.4 shows a set of a deposited Au electrode. Tails were designed to

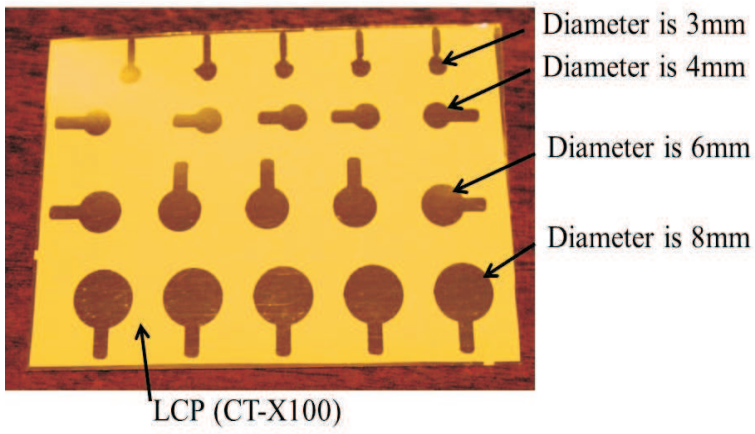

Figure 3.4: Deposited Au specimens before wire connection.

provide a contact out of the electrodes without affecting their surface. After wire connection, as shown in Figure 3.5 tails were covered by an insulating glue so that only circular spaces were in effect for charge transfer through the electrochemical measurements.

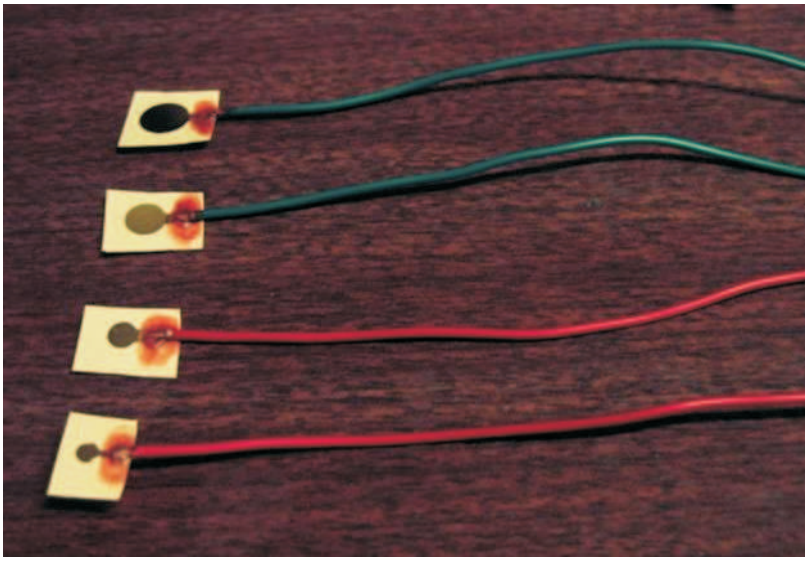

Figure 3.5: Au electrodes after wire connection and insulating the bare wires.

3.4 Characterization Techniques

3.4.1 Surface Characterization

The RMS surface roughness of deposited electrodes determine some properties in their electrochemical response to electrical stimulation, and hence, is of great importance. To determine the RMS surface roughness values, in this study, atomic force microscopy was used.

Atomic force microscopy (AFM) is known as one of the most multifaceted techniques of studying the surface morphology in sub-nanometer scale resolution. Therefore, it is very useful in determining the surface roughness.

The AFM commonly operates at two different modes: contact mode and tapping mode. Contact mode AFM is done by the tip touching and raster scanning across the specimen surface. However, some surface features may get destroyed due to the scraping between the tip and the specimen. In order to avoid any possible surface damage from the contact

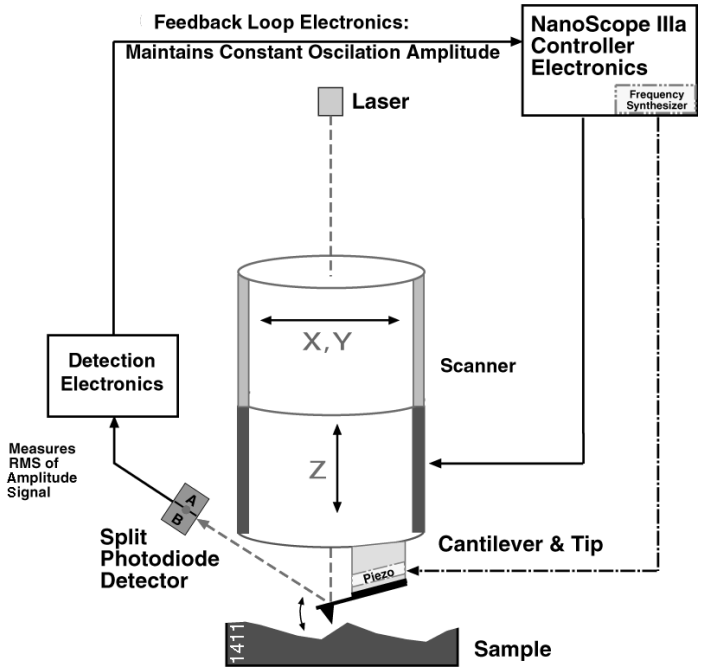

Figure 3.6: Schematic of tapping mode atomic force microscopy [42].

mode, tapping mode AFM was adopted in this study. Figure 3.6 shows a schematic of tapping mode AFM. In tapping mode, the cantilever with the attached tip is oscillated at or slightly lower than its resonant frequency with amplitude ranging typically from 20 nm to 100 nm [42]. As the tip taps on the specimen surface, a small piezoelectric element attached to the end of cantilever expands or contracts proportionally to an applied voltage. The piezoelectric is a part of the scanner which is capable of sub-angstrom resolution in x-, y- and z- directions. Therefore, a three dimensional image of the electrode surface topography is provided.

In this study, for surface roughness measurement, an AFM from Veeco (ICON) was used. Silicon tip in tapping mode was utilized over a scanning area of 500×500 nm^2 and 1×1 μm^2 and 5×5 μm^2. All measured RMS surface roughness values were averaged from scanning three different areas of each electrode with standard deviation of much less than

10% of each raw value.

3.4.2 Interface Characterization Techniques

In addition to surface measurements, the electrode/electrolyte interface is the next place to monitor for understanding the differences in electrodes behaviors. The interface characterization is also critical since it allows understanding the charge transfer mechanisms at the electrode/electrolyte interfacial regions in conditions similar to those of neuromuscular electrical stimulation. In this study two main interface characterization techniques were performed:

1. Electrochemical impedance spectroscopy (EIS),
2. Cyclic voltammetry (CV).

For implementing both electrochemical measurements, the same set up was used. All electrochemical measurements were implemented in a 0.1-molar phosphate buffered saline (PBS) solution at room temperature. A standard, three-electrode-cell set up was used as the configuration. A schematic representation of this experimental set up is presented in Figure 3.7.

As shown in Figure 3.7 and as its name suggests, the set up consists of three electrodes. The electrode, which is being studied or where the electrochemical processes should take place, is called the working electrode (WE). The second electrode, which closes the circuit for the current to flow, is called the counter electrode (CE). The third one, that measures the voltage between the electrolyte and WE, is called the reference electrode (RE). Reference electrode should keep a stable potential. To keep the potential stable, the concentrations of any ionic species involved in the electrode reactions should be held at a fixed value.

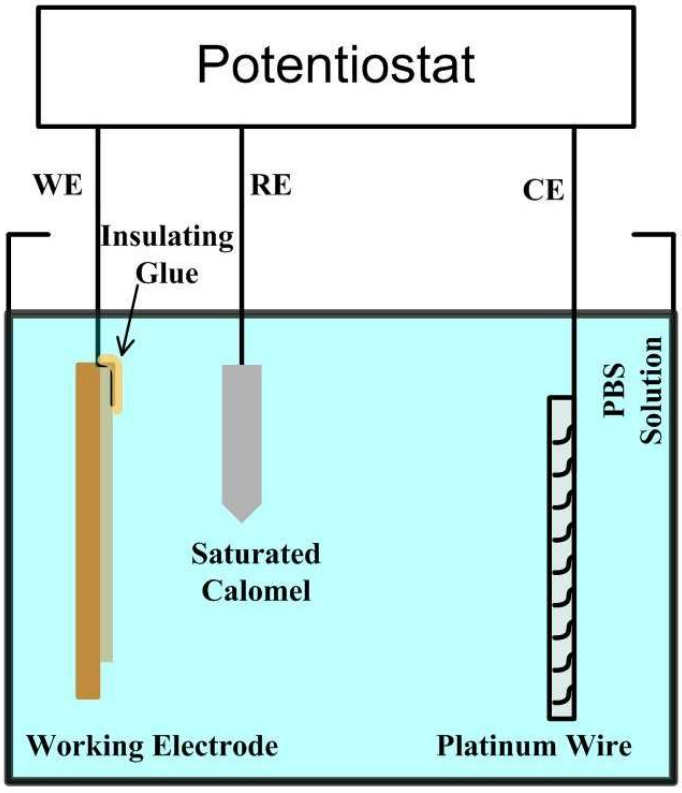

Figure 3.7: Schematic of electrochemical measurements set-up.

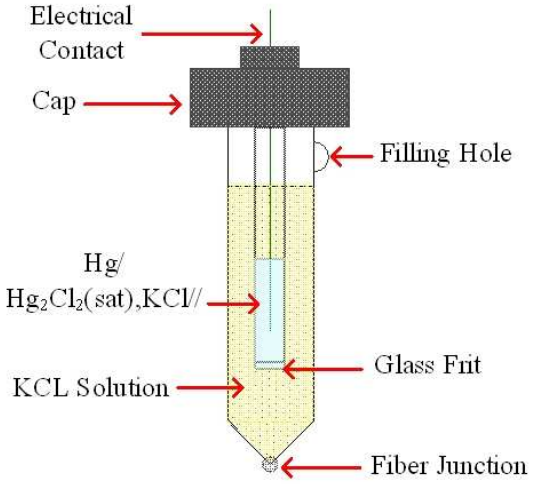

Figure 3.8: Calomel reference electrode. The calomel electrode is an Hg/HgCl system with a fiber junction. The electrode is refillable with saturated KCl. The porous frit functions as a salt bridge.

The most common way to do so is using a redox system involving a saturated solution of an insoluble salt of the ion. For this case, as shown in Figure 3.8, the saturated calomel electrode (SCE) is used, that is based on the reaction of mercury, mercury (l) chloride.

In this project, as Figure 3.7 presents, the measurements were implemented through the following set up:

1. Working electrode was connected to the Au, Ti and Pt films of the flexible electrode through an external wire.

2. A calomel reference electrode was immersed in an electrolytic solution in a glass container, as previously described.

3. The counter electrode was connected to a platinum wire with a glass rod as the support in the cell.

4. Electrochemical impedance spectra and cyclic voltammograms were taken with an electrochemical interface (Gamry Potentiostat) controlled by a computer with Gamry Framework and Echem Analyst software for both EIS and CV.

The following sections describe the details of interface characterization techniques that were performed in this study.

Electrochemical Impedance Spectroscopy

Electrochemical impedance spectroscopy (EIS) has attracted a lot of interest in electrode characterization in recent years [1–3, 13, 20, 40, 43–45]. EIS provides a strong tool to determine the electrode processes and complex reactions at electrode/electrolyte interfacial regions. Through EIS, a periodic small amplitude alternating current (AC) signal is applied to the cell, and its response is studied. This response includes information regarding the interface and reactions taking place there. Since the measurements are performed at different ac frequencies, it is called electrochemical impedance *spectroscopy*.

For EIS measurements, basically a sinusoidal voltage signal is applied between working electrode (WE) and reference electrode (RE), and current is measured between counter electrode (CE) and working electrode. From the known voltage and measured currents, impedance is calculated. As shown in the set up of Figure 3.7, there are two junctions: WE/Electrolyte junction and CE/Electrolyte junction. Therefore applied potential to the system is distributed as Equation 3.1:

$$U = U_{WE} + U_{CE} \tag{3.1}$$

Where U_{WE} and U_{CE} are the voltages across WE/electrolyte and CE/electrolyte junctions respectively, and since electrodes are highly conductive and electrolyte impedance

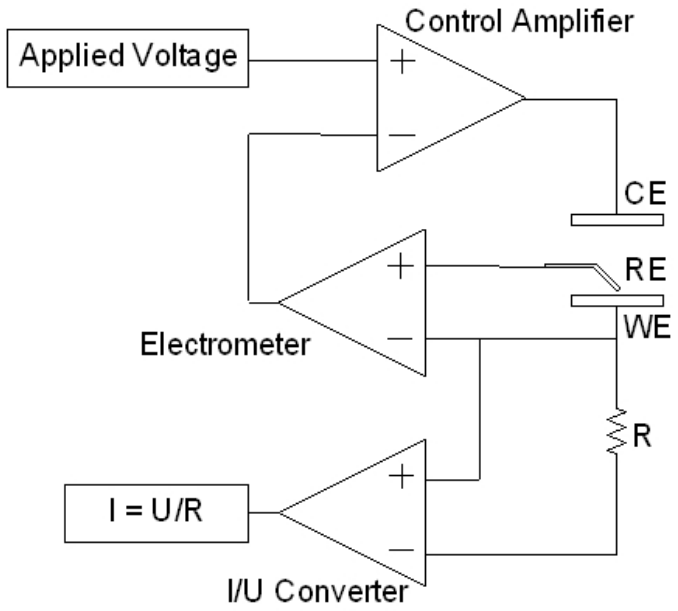

Figure 3.9: Schematic of potentiostat working principle [46].

is relatively small (as measured in the model), the losses in the bulk of solid electrode and electrolyte are negligible. Although only WE/electrolyte junction is desired to get the applied potential, CE/electrolyte junction also gets some part of applied potential. In this case, to study the impedance, the voltage between the sample and solution (U_{WE}) should be under control to measure the change in resulting current. However, the current stimulates electrochemical reactions also at the CE/electrolyte interface varying U_{CE} in time.

Since the total applied voltage is constant, the instability of U_{CE} changes the value of U_{WE}. Consequently, controlling the applied voltage signal does not guarantee the voltage constancy measured between the sample and the RE. To avoid this problem, potentiostat is used. A potentiostat controls the voltage between the working electrode and the reference electrode directly. The working principle of a potentiostat is shown in Figure 3.9.

Electrometer measures the actual WE-RE voltage by a differential amplifier. If the

state of counter electrode (U_{CE}) varies in time changing the value of U_{WE}, the second differential amplifier (control amplifier) comparing U_{WE} to the applied voltage, detects a change and adjusts the voltage to the cell until the actual and the applied voltages are equal. Cell current is achieved through measuring the voltage drop across the resistor R by I/U converter.

To perform EIS in this research, an alternating current excitation voltage of $10\ mV$ in amplitude was applied to measure the impedance between working electrode and electrolyte over a frequency range of $0.1\ Hz$ to $100\ KHz$. The sampling rate was $10\ steps/decade$ which was the same for all experiments. This sampling rate is of great importance due to the following explanation: It is considered that the period of applied signal should be lower than the time constant of double layer capacitor. This will guarantee that at the end of the pulse, before the next pulse, charge on the double layer capacitor discharges moving the electrode potential towards the open circuit potential. If the time between two pulses is long enough, electrodes potential will approach its open circuit value. This length depends on the time constant for discharge of the double layer capacitor. As in Equation 3.2, this value is the product of double layer capacitance and electrolyte resistance. τ_{dl} is in the range of microseconds for electrodes in macroscopic size. Smaller size of electrodes shifts this limit towards nanoseconds.

$$\tau_{dl} = R_e.C_{dl} \tag{3.2}$$

However, if a second pulse arrives before the electrode is fully discharged, *i.e.*, τ_{dl} is smaller than the period of stimulating AC signal, then the potential at the start of the second pulse is more positive than the open circuit potential. This could cause anodic faradaic reactions such as electrode corrosion.

As discussed in chapter two, one of the primary limiting factors in the application of

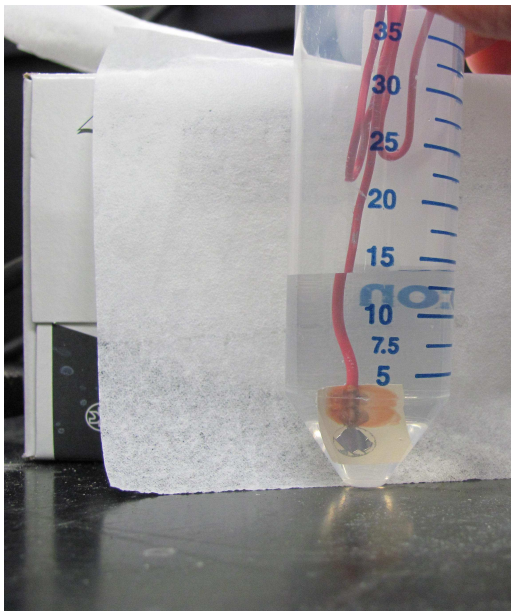

Figure 3.10: Electrode immersed in PBS solution inside the cylindrical plastic container for the long-term evaluations.

implanted stimulation electrodes was the necessity of being electrochemically stable in long-term applications. In order to address this issue, the fabricated electrodes longevity was evaluated. For this purpose, their interfacial impedance was measured at many time stages while there were kept immersed in PBS solution into cylindrical plastic containers with conical bottom. Figure 3.10 shows how the samples were kept through the 42-day experiments. These containers were used to avoid the contact of top part of the copper wire with the PBS solution. The measurements took place after three days, and then weekly from seven days, fourteen, twenty one, twenty eight, thirty five and finally forty two days of immersing which was the end of the sixth week. The measurement stopped after the sixth week because of the electrochemical impedance response of the electrodes by that time. After the end of EIS measurements, RMS surface roughness of electrodes were measured again and compared with their values before the long-term studies.

Cyclic Voltammetry

Cyclic voltammetry (CV) is one of the most widely used techniques for studying electrochemical processes of electrode/electrolyte systems [40,47]. In cyclic voltammetry, a linear ramp potential is applied to the electrode. This potential sweeps between two set values(E_1 and E_2) at a fixed rate. The rate of this ramping is called the experiment's scan rate ν (V/s). The potential sweep is applied between the working electrode and the reference electrode starting from E_1. When cyclic voltammetry reaches E_2, the working electrode's potential is reversed and swept back to E_1, still at the rate of ν. During this scan, the current is measured between the working electrode and the counter electrode. This data is then plotted as current (i), and sometimes current density (i/A), versus potential (E). The plot is called cyclic voltammogram.

Cyclic Voltammograms can help observe possible oxidation, reduction and electrolysis reactions. Characteristic peaks or shoulders at some potentials on CV curves are evidence of electrochemical processes at those potentials, and thus are used to characterize the electrodes.

In addition to electrochemical reactions assessment, cyclic voltammetry is used to investigate the charge delivery capacity (CDC) of electrodes. Charge delivery capacity is the total quantity of charge that may be injected into, transferred through or stored in the electrode reversibly. This include double layer capacitance, pseudocapacitance, or any reversible faradaic processes. In neuromuscular electrical stimulation, high CDC electrode is demanded. A high CDC electrode can handle a relatively large amount of injected charge without causing any damage to either the tissue, which is stimulated or the electrode itself. In addition, higher value of CDC would require smaller area to transfer certain amount of charge. Since practical applications require miniaturized electrode geometry to

control a large number of different muscles, high charge delivery capacity material is demanded [13,25,26,35]. This CDC value depends on the electrode's material, the size, shape and deposition condition of electrode and parameters of electrical stimulation waveform.

In this study, the CV was recorded applying a scan rate of $100\ mVs^{-1}$. This scan rate is the highest scan rate at which potentiostat is able to run CV [48]. Hence, it was the closest frequency we could get to real stimulation. CV measurements in this study are acquired from the second cycle. To avoid the electrolysis of water the potential between the working electrode and the reference electrode was swept in the range of $-0.6\ V$ to $0.8\ V$. Cyclic voltamograms were acquired for each electrode. From CV curves, CDC value was calculated by integrating the current with respect to voltage, over the voltage sweep range of $-0.6\ V$ to $0.8\ V$. In other words, CDC is obtained by measuring the enclosed area inside the cyclic voltammoram graph, as shown in Equation 3.3:

$$CDC = \frac{1}{\nu}\int_{E_c}^{E_a} |i|\ dE \tag{3.3}$$

Where E is the electrode potential (V), i is the measured current density ($mA\ cm^{-2}$), ν is the scan rate ($V\ s^{-1}$), and E_a and E_c are the anodic and cathodic potential limits (V). Consequently CDC was calculated as $mC\ cm^{-2}$.

3.5 Interface Model

As discussed and measured through electrochemical impedance spectroscopy and cyclic voltammetry tests, some charge transfer reactions occur within a very narrow region close to the electrode surface at electrode/electrolyte interface. In this interfacial region, the charges on the electrode attract oppositely charged ions in the electrolyte. This results in

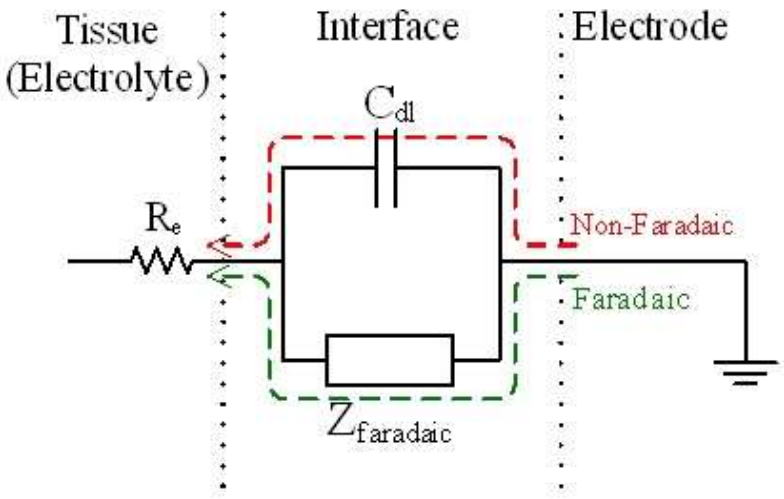

Figure 3.11: Schematic of electrode/electrolyte interface showing different pathways of charge transfer [40].

an ion concentration at the electrode electrolyte interface. Since there is a small charge separation distance between charges in the electrode and in the electrolyte (about 20 nm), a capacitive behavior is implied [4, 40]. This double layer capacitance can be increased with higher electrode potentials or higher ion concentration levels at the electrode surface. Figure 3.11 shows one of the most accepted models for this interfacial charge transfer behavior [26, 45, 49].

R_e and C_{dl} are the electrolyte resistance and the double layer capacitance, respectively. Double layer capacitance shows the electrode ability to inject charge in the electrolyte (body tissue) without transferring electrons. The two pathways noted by dashed lines represent the capacitive and faradaic processes of charge injection from the electrodes towards the tissue. $Z_{faradaic}$ represents the reduction/oxidation processes of faradaic charge transfer between the electrode and electrolyte.

To analyze EIS data and basically to investigate the charge transfer parameters, based on

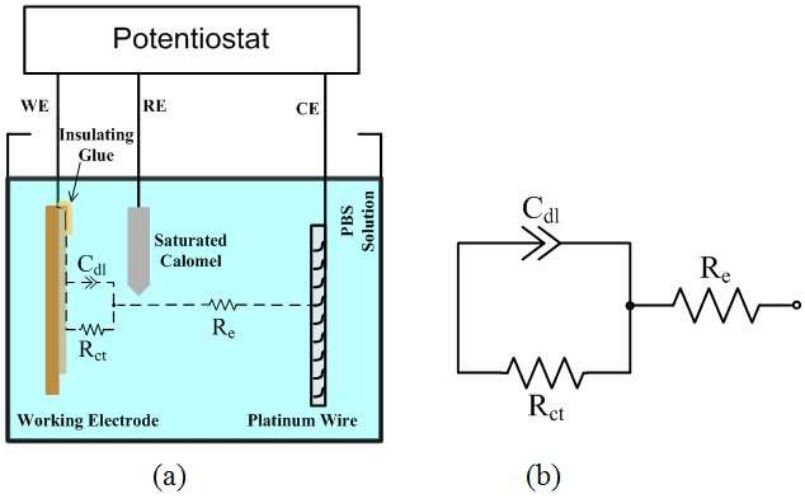

Figure 3.12: (a) Schematic set-up for electrochemical measurements, and (b) equivalent circuit model of electrode/electrolyte interface.

the explanations of Figure 3.11, an equivalent electrical circuit model of electrode/electrolyte interface is used. Figure 3.12 shows the Randles cell which models the electrochemical impedance of electrode/electrolyte interface and the cell model that is formed in the set up used in this study.

The Randles cell model is an equivalent circuit of the system consisting of an interface constant phase element (CPE) modeling the double layer in parallel with a charge transfer resistance (R_{ct}) that are in series with the electrolyte resistance (R_e). CPE is an intuitive element that is introduced since double layer is not a pure capacitor, but an phase element with imperfect capacitive behavior in nature. CPE impedance is given by Equation 3.4, as :

$$Z_{CPE} = \frac{1}{K(j\omega)^{\beta}} \tag{3.4}$$

Where K is the magnitude of the CPE, and β a constant that varies between zero and one. The case $\beta = 0$ describes a pure resistor and $\beta = 1$ describes an ideal capacitor. It should be noted that the surface and volume resistivities of the LCP are $10^{14}\ Ohm$ and

$10^{13}\ Ohm.m$, respectively. These are much higher than those of metal films while being parallel to them. Therefore, the influence of current flow through the LCP is negligible compared to that of electrodes.

To investigate the impedance spectra, model parameters were then fit to the experimental results of EIS measurements. Equivalent parameters were determined with ZView software from experimental data. ZView software makes use of nonlinear least square method for curve fitting.

From the model circuit, considering CPE as an ideal capacitor, shown as C_{dl}, its impedance is presented as:

$$Z(j\omega) = (R_e + R_{ct}) \left(\frac{1 + j\omega(\frac{R_e\ R_{ct}\ C_{dl}}{R_{ct} + C_{dl}})}{1 + j\omega(R_{ct}\ C_{dl})} \right) \tag{3.5}$$

At very high frequencies, the effect of R_{ct} may be neglected because the system functions like a high-pass filter. The cut off frequency of this high-pass filter, which is defined as the frequency at the interception point of rising slope tangent with the line of constant impedance, is obtained by Equation 3.6, as:

$$f_c = \frac{1}{2\ \pi\ R_e\ C_{dl}} \tag{3.6}$$

At very high frequencies, C_{dl} dominates and the resulting interface impedance is approximately the electrolyte resistance, R_e, in series with C_{dl} . At very low frequencies, C_{dl} becomes an open circuit, resulting in an equivalent impedance of $R_e + R_{ct}$. On the other hand, the value of C_{dl} is proportional to the surface area ($C\ \propto\ A$). Since an electrode with a rougher surface exhibits a larger surface area, C_{dl} increases with the increase of surface roughness. Therefore, an electrode with a rougher surface is expected to exhibit a lower cut

off frequency. However, double layer is not a pure capacitor but a constant phase element with deviation from pure capacitive behavior and is calculated as Equation 3.4.

Considering the circuit shown in Figure 3.12 (b), if CPE could be considered as an ideal capacitor which makes the equations easier to study, its impedance is presented as Equation3.7:

$$Z(j\omega) = R_e + \frac{1}{(\frac{1}{R_{ct}} + j\omega C_{dl})} \tag{3.7}$$

Equation 3.7 could be rearranged into another form as:

$$Z(j\omega) = (R_e + R_{ct}) \left(\frac{1 + j\omega \, (\frac{R_e \, R_{ct} \, C_{dl}}{R_e + R_{ct}})}{1 + j\omega \, (R_e \, R_{ct})} \right) = (R_e + R_{ct}) \left(\frac{1 + j\omega\tau_1}{1 + j\omega\tau_2} \right) \tag{3.8}$$

Where τ_1 and τ_2 are the Bode characteristic time constants. To get the Bode magnitude plot $log_{10}(|Z|)$ is calculated from Equation 3.8:

$$log_{10}(|Z|) = log_{10}(R_e + R_{ct}) + log_{10}(|1 + j\omega\tau_2|) - log_{10}(|1 + j\omega\tau_1|) \tag{3.9}$$

To obtain the Bode magnitude plot, each term of Equation 3.9 can be considered independently and then their sum may be easily constructed. Each term of $log(|1 + \tau|)$ has two limits:

$$\begin{cases} log_{10}(1 + j\omega\tau) = 0, & \text{When } \omega\tau \ll 1 \quad \Rightarrow \quad \omega \ll \frac{1}{\tau}, \\ log_{10}(1 + j\omega\tau) = log_{10}(\omega) + log_{10}(\tau), & \text{When } \omega\tau \gg 1 \quad \Leftarrow \quad \omega \ll \frac{1}{\tau}. \end{cases} \tag{3.10}$$

Second equation corresponds to a straight line with a slope of one and intercept of $log_{10}(\tau)$. The graph corresponding to these lines is shown as Figure 3.13. In reality, however, the slope is slightly different as C_{dl} is not an ideal capacitor but a constant phase element, and its impedance is given by Equation 3.4.

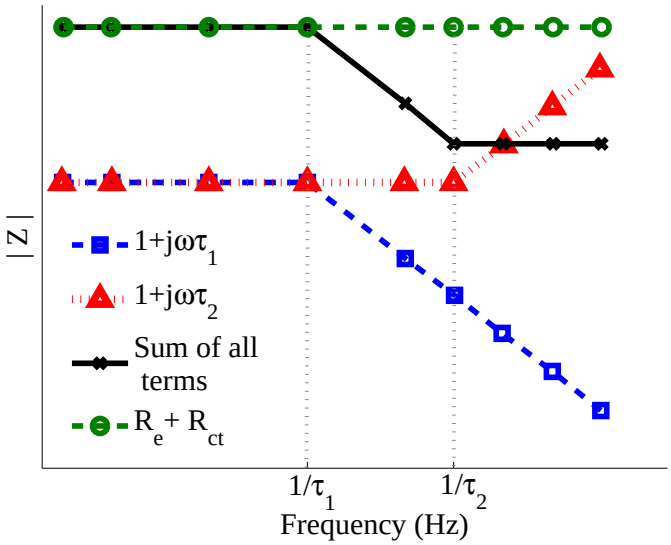

Figure 3.13: Bode magnitude plot for the model circuit in Figure3.12(b) using Equation 3.9. The black curve is the sum of all three contributions which suggests the general form of interfacial impedance magnitude spectra [50].

Therefore, in this research, model parameters were extracted form fitting experimental EIS data to the equivalent circuit. The parameters were then verified with AFM results and used to explain the electrodes functionalities and evaluate the their performance.

Chapter 4

Interfacial Impedance Studies

In this Chapter, we provide the reader with the results of our experiments regarding the electrochemical impedance of the electrode/electrolyte interfacial regions. The chapter begins with the measurement results of RMS surface roughness for all the specimens. It is followed by elucidating the size, material and deposition pressure dependence of interfacial impedance. Next, the results of impedance studies in long term evaluations of electrodes are stated. Electrodes performances are investigated based on their impedance magnitude spectra and the equivalent model parameters. The results are explained based on the theoretical justifications which were discussed in previous chapters.

4.1 Measurement of Surface Roughness

Table 4.1 shows the RMS surface roughness value of each film on LCP substrate and also on silicon (Si) substrate. RMS surface roughness of electrodes on Si substrate is also measured because Si is known for providing electrodes with the smoothest surface. It should be noted that for the fabrication of electrodes on Si and LCP substrates the identical conditions were applied. Therefore, Si substrate is used as a scale of how rough the films on this LCP are. Since LCP offers rougher surface than Si, it is expected that LCP provides electrodes with rougher surfaces than Si substrate.

Table 4.1: RMS values of surface roughness of all samples obtained from AFM.

Films	**RMS Surface Roughness (much less than** 10%**)** $500 \times 500\ nm^2$	$1 \times 1\ \mu m^2$	$5 \times 5\ \mu m^2$
Au on Si	2.04 nm	2.16 nm	2.23 nm
Pt on Si	2.88 nm	2.98 nm	3.09 nm
Ti on Si	3.85 nm	4.32 nm	4.35 nm
Ti on Si- Lower Pressure	4.22 nm	4.71 nm	4.82 nm
Au on LCP	2.12 nm	3.18 nm	7.75 nm
Pt on LCP	2.87 nm	3.44 nm	5.70 nm
Ti on LCP	3.58 nm	4.49 nm	6.57 nm
Ti on LCP- Lower Pressure	4.93 nm	5.49 nm	8.81 nm

Figure 4.1 shows the AFM image of Pt sample deposited on (a) Si substrate and (b) LCP substrate from scanning a $5 \times 5\ \mu m^2$ area. As also shown by Table 4.1, it is observed that Pt deposited on LCP has relatively rougher surface than Pt deposited on Si at the same deposition conditions. AFM images of Pt sample on Si and LCP substrates are shown as

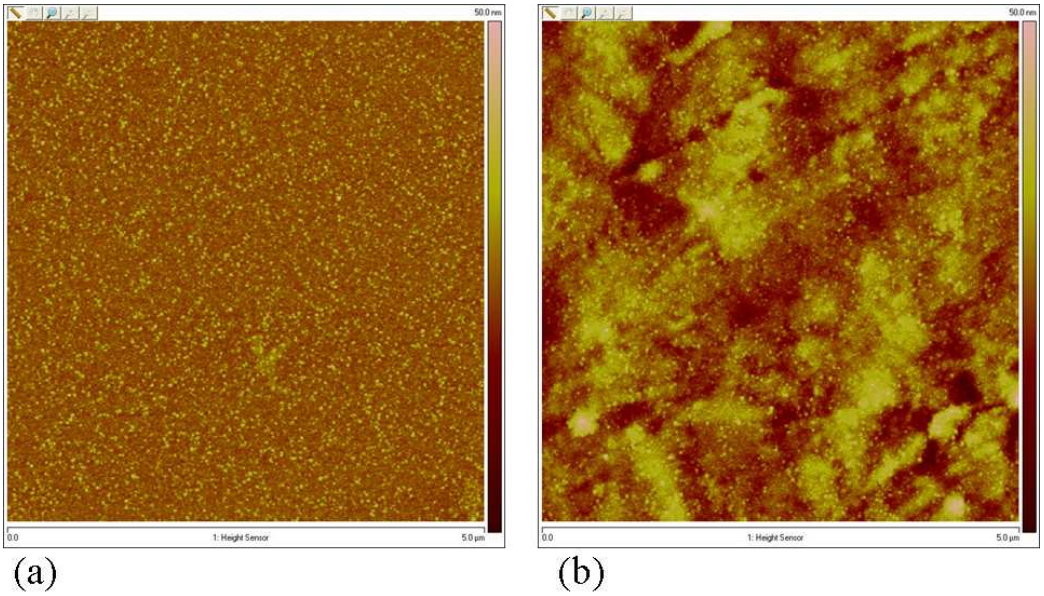

Figure 4.1: AFM images of Pt electrodes through a scan area of $5 \times 5 \mu m^2$ on (a) Si substrate and (b) LCP substrate.

examples as AFM images of other films suggest a similar message. Figure 4.1 and the AFM data confirm this idea except for the scan area of $500 \times 500\ nm^2$. For the scan size of $500 \times 500\ nm^2$ some measurement errors are detected for the cases of Pt and Ti samples. The reason is that the scan area was so small and failed in providing an appropriate sample. This problem was solved by looking at larger scan areas of $1\ \mu m^2$ and $5 \times 5\ \mu m^2$. The data proposes that Au electrodes offer the smoothest surface followed by Pt and Ti, respectively. However, it should be noted that for Au on LCP sample of $5 \times 5\ \mu m^2$, due to some after deposition scratches that occurred during sample handling, the measured surface roughness is larger than the real surface roughness of Au. This fact is verified by the results from $500 \times 500\ nm^2$ and $1 \times 1\ \mu m^2$ scan areas.

As Table 4.1 and Figure 4.2 suggest, higher values of surface roughness are obtained for Ti films deposited under lower pressure compared to those Ti films deposited at higher pressure.

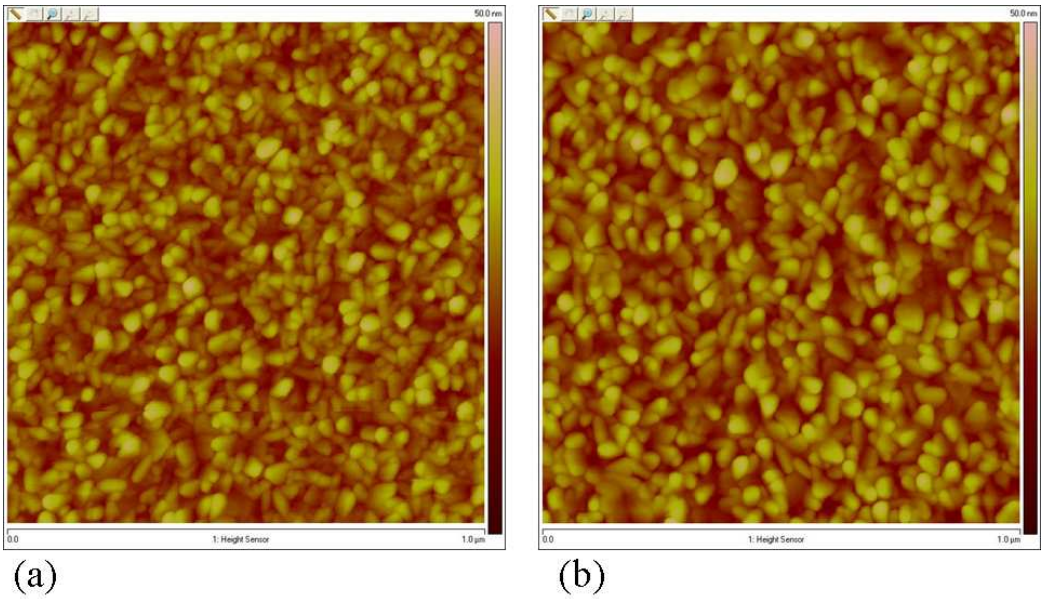

Figure 4.2: AFM images of Ti electrodes on Si deposited at (a) $10^{-6}\ Torr$ and (b) lower pressure of $3 \times 10^{-8}\ Torr$.

As mentioned earlier and according to the literature [3, 40], higher surface roughness increasing the real surface area results in larger values of double layer capacitance. According to equation (3.6), the larger value of double layer capacitance causes lower cut off frequency (f_c). The location of f_c together with the value of β, which sets the slope of impedance magnitude spectra, define the electrode/electrolyte conductivity (or impedance magnitude) in low frequencies, and hence are significant to assess.

Therefore, Au electrodes with the smoothest surface are expected to exhibit the highest f_c, followed by Pt, Ti and Ti deposited at lower pressure. This is verified based on Figure 4.3. Figure 4.3 demonstrates cut off frequencies of each electrode at all diameter sizes. The cut off frequency of each electrode is derived from the electrodes electrochemical impedance magnitude spectra.

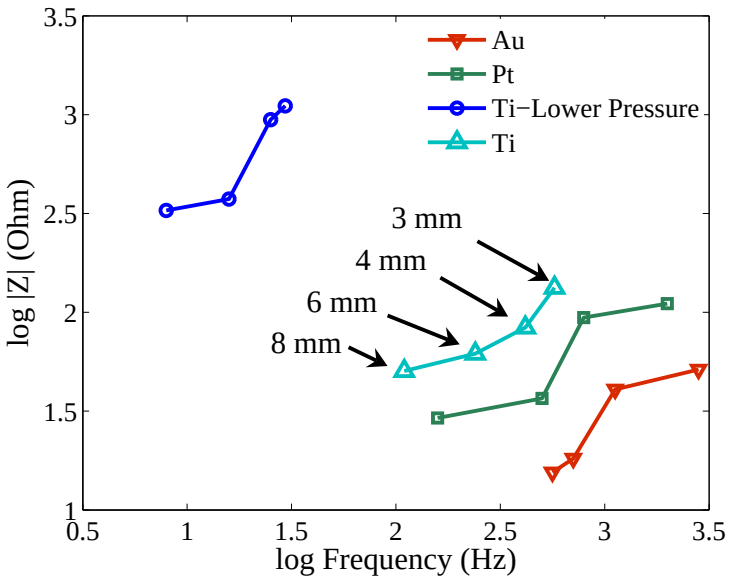

Figure 4.3: Quantitative look at the cut off frequencies of each film at 3, 4, 6 and 8 mm diameter sizes.

4.2 Size Dependence of Interfacial Impedance

Figure 4.4 represents the Bode magnitude plots of measured EIS from Pt, Au, and Ti films deposited under the same conditions. As the area diameter of electrode increases, the impedance magnitude decreases for all materials at all frequencies.

To make the interpretation easier, Figure 4.5 plots the impedance magnitude of each film versus the size at three main frequencies in or close to neuromuscular electrical stimulation frequency range. Neuromuscular stimulation is performed at frequencies below 10 KHz. As it shows, with the increase of electrode size, the impedance magnitude decreases for all electrodes at all frequencies. The identical effect of electrode area on impedance is reported for Au electrodes on PI substrates as shown in Figure 4.6 [1]. Au electrodes in their study were prepared through e-beam evaporation technique on PI substrate. To improve the contact of Au to PI, a Ti adhesion layer was used (the thickness of

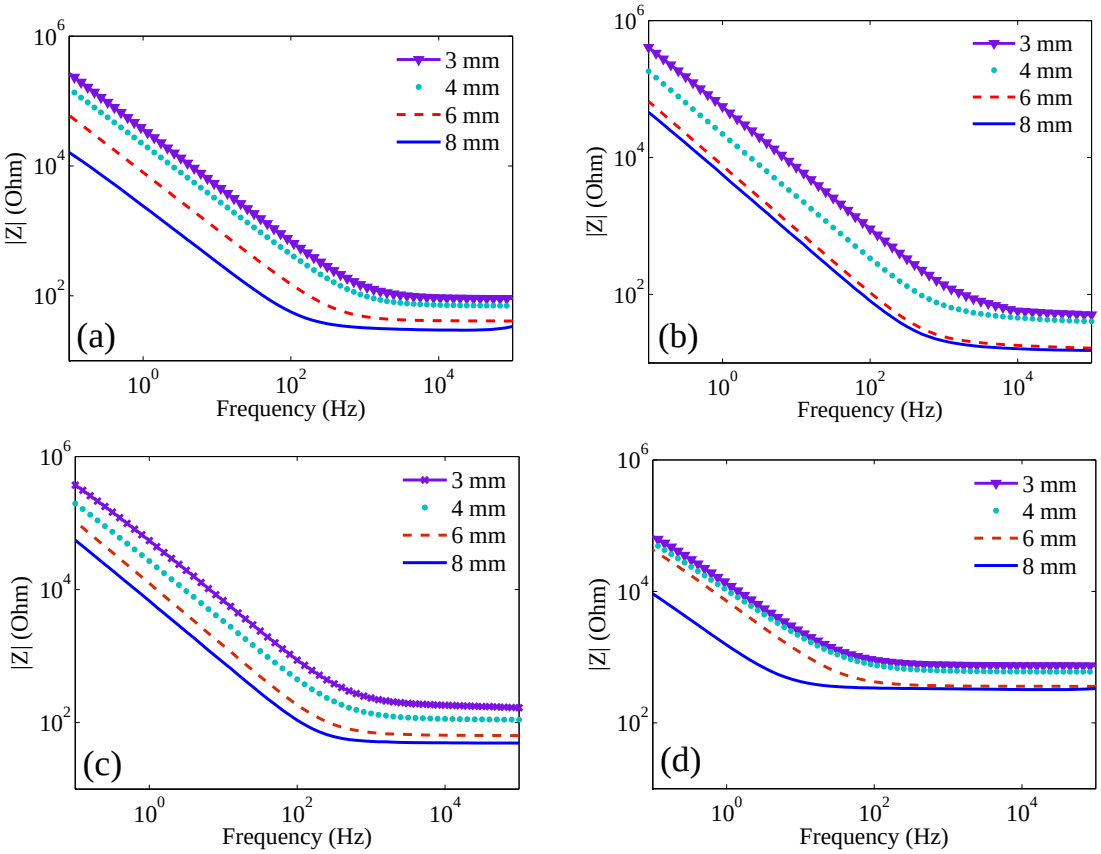

Figure 4.4: Impedance magnitude spectra of (a) Pt, (b) Au, (c) Ti and (d) lower pressure deposited Ti electrodes of 3, 4, 6 and 8 mm diameter size.

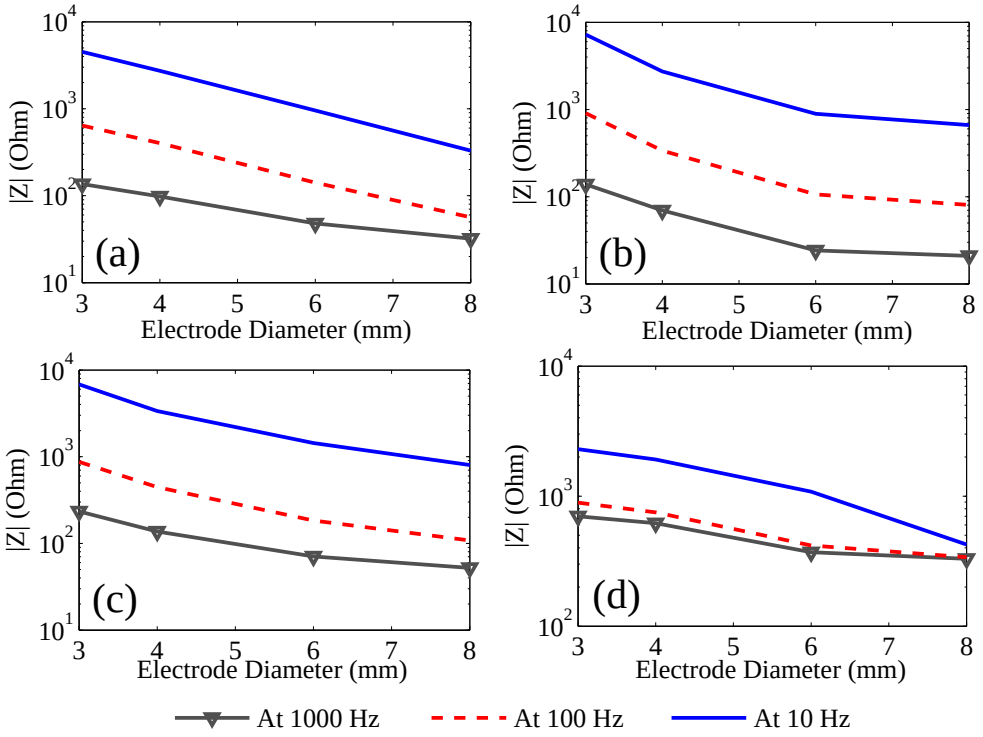

Figure 4.5: Impedance magnitude versus electrode size for (a) Pt, (b) Au,(c) Ti electrodes and (d) Ti deposited at lower pressure. The curves are plotted at three different frequencies.

adhesion layer was not mentioned). However, to the best of our knowledge, for Pt, Ti and lower pressure deposited Ti, such comparative study of size dependence was not reported.

The values of the circuit model parameters obtained by fitting the impedance experimental data to the equivalent circuit model (as discussed in Chapter 3 through Figure 3.12) are shown in Table 4.2. From Table 4.2, it is inferred that with the decrease of electrode area, the magnitude of CPE (K) decreases while R_{ct} and R_e increase. We do not observe any β dependence of size in the results. Hung et. al [40] and Brett [43] also mentioned the same relation of electrochemical biosensors size with K and R_{ct}. As also shown in Figure 4.3, with the decrease in electrodes size, cut off frequencies shift toward higher frequencies. As discussed in previous section, this shift of cut off frequencies with

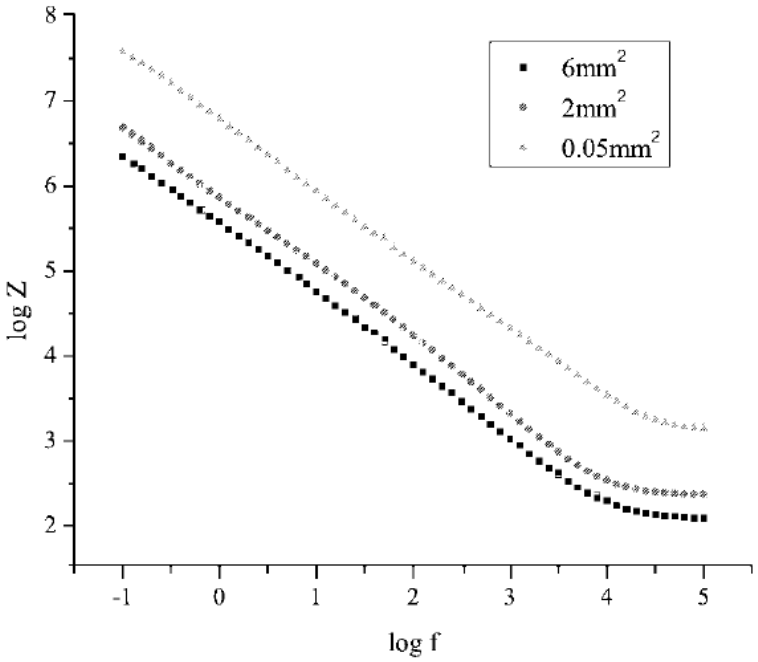

Figure 4.6: Impedance magnitude versus electrode size for Au electrode of three different areas in 0.01 M PBS solution from McAdams *et. al* study [1].

size decrease is due to the fact that double layer capacitance is directly and charge transfer resistance is reversely proportional to the surface area of electrode/electrolyte interface ($f_c \propto C_{dl}^{-1}$ and $C_{dl} \propto A$ and $R_{ct} \propto A^{-1}$). Thus, for each material, the electrode with $3\ mm$ diameter has the highest cut off frequency followed by $4, 6$ and $8\ mm$ diameter samples.

4.3 Material Dependence of Interfacial Impedance

In addition to the size of stimulation electrodes, their material also has influence on the interfacial electrochemical impedance. Figure 4.7 shows a comparison of impedance magnitude of different materials with the same sizes. The important difference in impedance spectra of these metallic films in neuromuscular stimulation frequency range below 250 Hz, is the location of f_c and the value of β. At frequencies lower than f_c, the electrode

material shows the capacitive behavior with a rising slope of $-\beta$, as discussed in Equations 3.6 and 3.8. Compared to Pt and Ti, Au proposes the highest f_c, which is due to its smoothest surface. This high f_c along with its high value of β provides Au with the highest impedance magnitude in frequencies lower than its f_c. Despite the higher f_c of Pt compared to Ti, it offers lower impedance in the range of 1-250 Hz, which occurs because of its lower β values. At frequencies above their f_c, similar values of impedance magnitudes are suggested for Pt, Au and Ti. Figure 4.8 shows the electrochemical impedance spectra for the four electrodes that Tandon *et. al* [2] studied. Similar to our results, it is observed that the material with largest magnitude of CPE, demonstrates the lowest cut off frequency in electrochemical impedance spectra. In addition, they reported that the main shape of the impedance spectra is alike for all the measured materials which is confirmed through our results, as shown in Figure 4.7.

4.4 Deposition Pressure Dependence of Interfacial Impedance

To study the effect of deposition pressure on the Ti electrodes performance, two sets of Ti samples were prepared. One set underwent an identical procedure to Pt and Au. The other set had all parameters the same except for the deposition pressure. The second set of Ti was deposited under lower pressure of 3×10^{-8} Torr. These two Ti sets of electrodes are compared through their electrochemical performances.

According to Table 4.1, for those Ti samples deposited under lower pressure of 3×10^{-8} Torr, rougher surfaces are observed compared to those deposited under higher pressure of

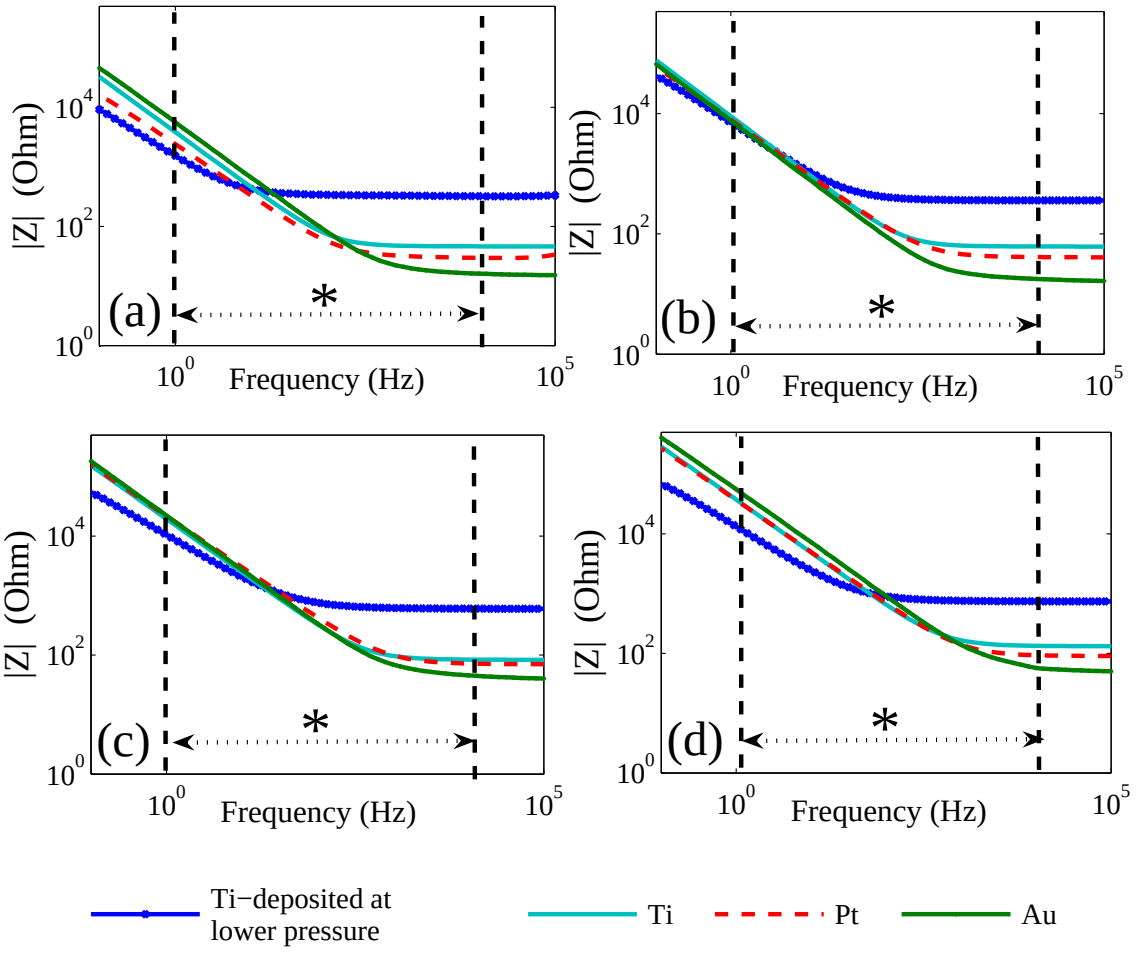

Figure 4.7: Impedance magnitude spectra of Pt, Au, and Ti electrodes of (a) 8, (b) 6, (c) 4, and (d) 3 mm diameter size. Note that * shows the neuromuscular stimulation frequency range.

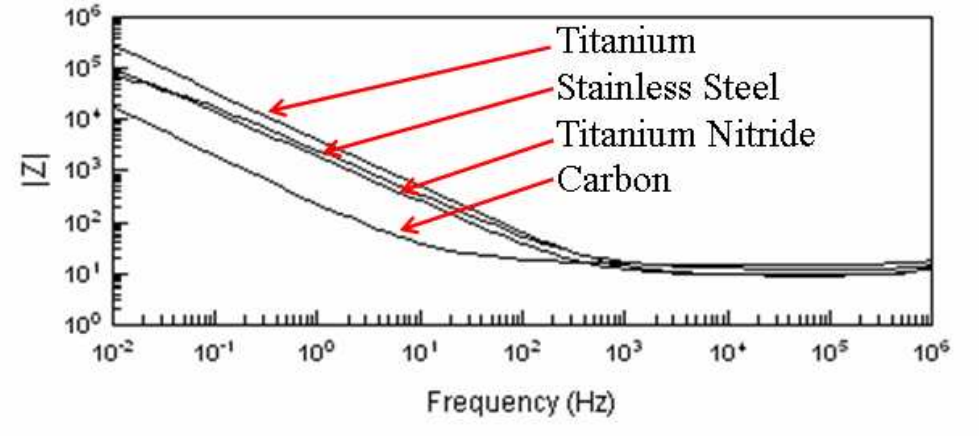

Figure 4.8: Impedance magnitude spectra of titanium, stainless steel, titanium nitride and carbon from Tandon *et. al* study [2].

1×10^{-6} Torr. This rougher surfaces of lower pressure deposited Ti, increase the real surface area of these electrodes. As discussed earlier, electrodes with larger real area provide larger double layer capacitance. Therefore, the electrodes that are deposited under lower pressure imply higher magnitudes of CPE. This is confirmed by Table 4.2. As Table 4.2 proposes, these low pressure deposited Ti electrodes offer larger magnitudes of double layer capacitance (K) but smaller values of β. The larger values of double layer capacitance offer lower cut off frequencies, compared to the Ti films deposited under higher pressure of 1×10^{-6} Torr. This shift of cut off frequency is observed in Figure 4.3. This results in their higher conductivity (lower impedance magnitude) in low frequencies that is of our interest.

However, according to Lee *et. al* study [3], if the working pressure is lower than a material pressure threshold, poor electrochemical properties would be observed. On the other hand, very high pressure could result in adhesion problems such as delamination between the conducting material and polymer substrate. Hence, they concluded that the working pressure has to be optimized in order for electrodes to propose the desired performance (see Figure 4.9). It should be noted that as explained in Chapter 2, they used radio

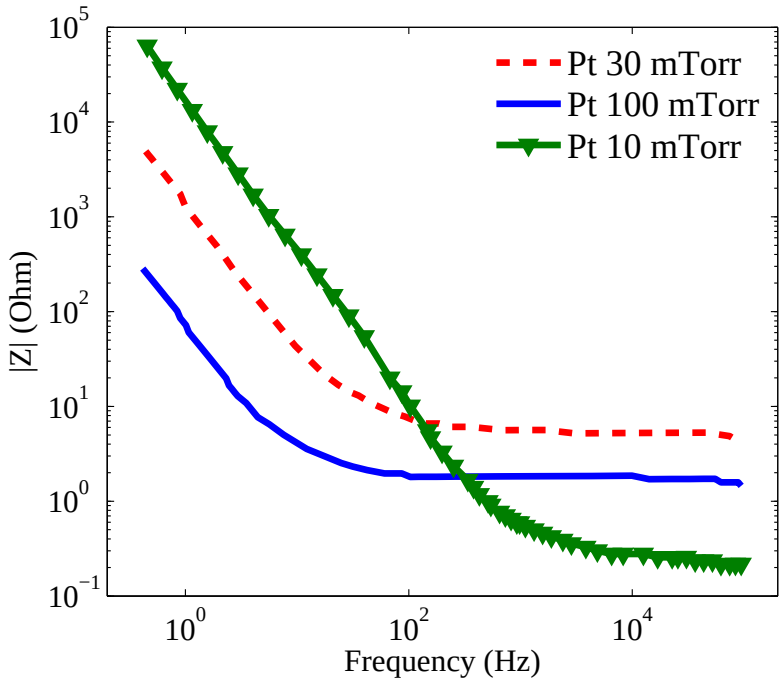

Figure 4.9: Impedance magnitude spectra of Pt electrodes deposited at different sputtering pressures from Lee *et. al* study [3].

frequency sputtering technique for the fabrication of nerve electrodes, which was different from our fabrication technique.

However, it should be noted that this behavior of two sets of Ti electrodes cannot be explained only by using the pressure dependent change in surface roughness, and hence, further study is suggested in this area.

Consequently, as demonstrated in Table 4.2, it is found that R_e and R_{ct} decrease as the size of electrodes increases, while the double layer capacitance shows increase with the increase of electrode size. Further, Au electrodes with the smoothest surface (as observed in Table 4.1) propose the lowest double layer capacitance (CPE) followed by Pt, Ti and lower pressure deposited Ti, respectively. All in all, the AFM and measured impedance data demonstrate that not only the electrodes size and material, but also deposition pressure is one of the key factors that can influence the performance of stimulation electrodes, and

thus has to be considered in the fabrication process.

Table 4.2: Model parameters of all electrodes derived from EIS data.

Films	**Area Diameter**	$R_e(\Omega)$	CPE	β	$R_{ct}(M\Omega)$
Au	8 mm	17.85	3×10^{-5}	0.92	0.25
	6 mm	19.07	1.8×10^{-5}	0.93	1.2
	4 mm	48.87	7.8×10^{-6}	0.91	2.85
	3 mm	49.19	3.3×10^{-6}	0.88	5.08
Pt	8 mm	34	8.1×10^{-5}	0.89	2.1
	6 mm	51	2.1×10^{-5}	0.88	2.7
	4 mm	70	9.5×10^{-6}	0.86	3
	3 mm	90	5.5×10^{-6}	0.87	3
Ti	8 mm	55.2	5.2×10^{-5}	0.93	2.4
	6 mm	61.6	2.2×10^{-5}	0.93	2.4
	4 mm	67.9	1.1×10^{-5}	0.90	2.5
	3 mm	131.7	5.7×10^{-6}	0.89	2.6
Ti- Lower Pressure	8 mm	326	1.5×10^{-4}	0.84	10.3
	6 mm	351.1	1.9×10^{-4}	0.70	10.8
	4 mm	370.2	1.8×10^{-4}	0.72	10.9
	3 mm	383.7	1.8×10^{-4}	0.70	11

4.5 Long-term Studies of Interfacial Impedance

As discussed in Chapter 3, in addition to the interfacial impedance measurements of electrodes, EIS was utilized to investigate the longevity of the electrodes. To evaluate the long-term stability of each electrode type, they were immersed in PBS solution for 42 days at room temperature. Through this 42-day period, electrodes underwent electrochemical impedance spectroscopy measurements regularly. The measurements took place after three days, and then weekly from seven days, fourteen, twenty one, twenty eight, thirty five and finally forty two days, which was the end of the sixth week. After the end of EIS measurements, RMS surface roughness of electrodes were measured again and compared with their values before the long-term studies. Table 4.3 shows the RMS surface roughness of each electrode before and after the 42-day experiments.

Table 4.3: RMS Surface Roughness values of a $1 \times 1\mu m^2$ scan area before and after the 42-day experiments.

	RMS Surface Roughness	
Films	Before Experiments	After 42-Day Experminets
LCP	2.96 nm	5.43 nm
Au	3.18 nm	11 nm
Pt	3.44 nm	Due to high observable roughness not scanned
Ti	4.49 nm	6.03 nm

It offers that with elapsing time, each electrode type surface roughness increases due to water absorption. This increase of surface roughness is likely to cause R_{ct} to decrease.

Figures 4.10, 4.11 and 4.12 along with Tables 4.4, 4.5 and 4.6 show the electrochemical

impedance spectra and the circuit model parameters of Pt, Au and Ti electrodes through the 42-day experiments, respectively.

It is inferred from the figures that, by the end of experiments on the forty second day, the slope of the impedance spectra is decreased for all three electrodes. However, Au electrode shows more consistency in keeping the slope of its impedance spectra close to one. As discussed in Chapter 3, this slope decrease is a result of a drop in β value. Considering Equation 3.4, this drop in β value is a result of the diversion of double layer's capacitive behavior. This is quantitatively demonstrated by the model parameters in Tables 4.4, 4.5 and 4.6.

A significant drop in β value for both Pt and Ti is observed in long term evaluations. The causes of decrease in R_{ct} and β value, which are due to the change in capacitive and faradaic behaviors, require further study. Compared to Pt and Ti electrodes, Au samples offer the best stability by keeping β close to 1, which is a verification of capacitive behavior of double layer in the 42 days of observation. Except for a minor delamination at Pt electrode, no delamination was observed with Au and Ti films, illustrating the advantage of LCP over polyimide.

Hoffmann *et. al* also studied the long-term electrical behavior of 16 different transcutaneous electrode materials using EIS measurements for a duration of 10 days and came to similar conclusions [51]. Identical to our results, an increase in impedance magnitude was observed for all materials over the first days. After this initial increase, for the electrodes with polarizable metals such as Pt, Au and Ir, impedance stayed almost constant for the next week, when their experiments ended. However, they reported drops in the impedance magnitude with progressing time for some materials, such as silver, carbon and doped tin oxide. The reasons of these changes in electrodes stability were not discussed, though.

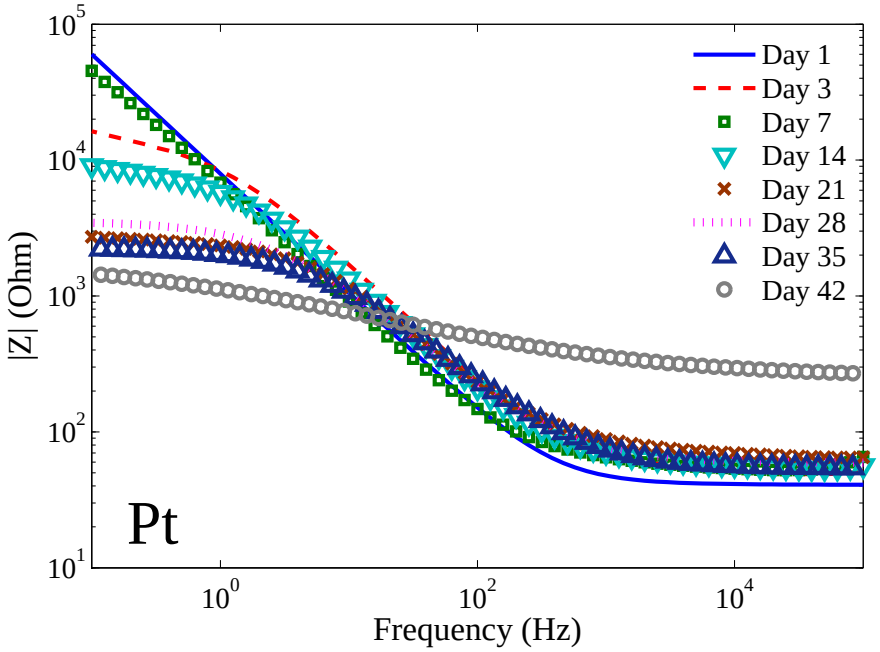

Figure 4.10: Impedance magnitude spectra of Pt electrode changing through the 42-day experimental period.

Table 4.4: Electrode/Electrolyte interface model parameters changing through 42 days of immersing Pt electrode in PBS solution obtained from fitting experimental data to model.

	Pt		
	$K(\times 10^{-5})$	β	$R_{ct}(k\Omega)$
Day 1	2.1	0.88	2700
Day 3	1.81	0.84	16
Day 7	2.11	0.84	13.4
Day 14	2.32	0.84	9.5
Day 21	2.78	0.80	3.4
Day 28	3.33	0.78	3
Day 35	2.90	0.78	2.1
Day 42	2.80	0.38	1.6

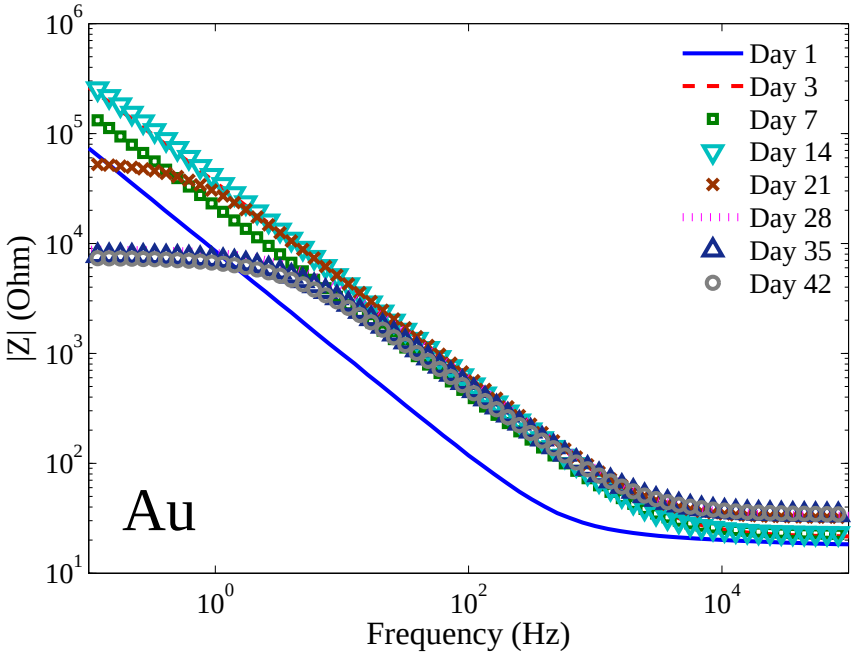

Figure 4.11: Impedance magnitude spectra of Au electrode changing through the 42-day experimental period.

Table 4.5: Electrode/Electrolyte interface model parameters changing through 42 days of immersing Au electrode in PBS solution obtained from fitting experimental data to model.

	Au		
	$K(\times 10^{-5})$	β	$R_{ct}(k\Omega)$
Day 1	1.80	0.83	1200
Day 3	5.40	0.84	1100
Day 7	0.94	0.86	1000
Day 14	0.42	0.92	849
Day 21	0.50	0.90	55
Day 28	0.59	0.88	8.8
Day 35	0.80	0.86	7.8
Day 42	0.90	0.85	7

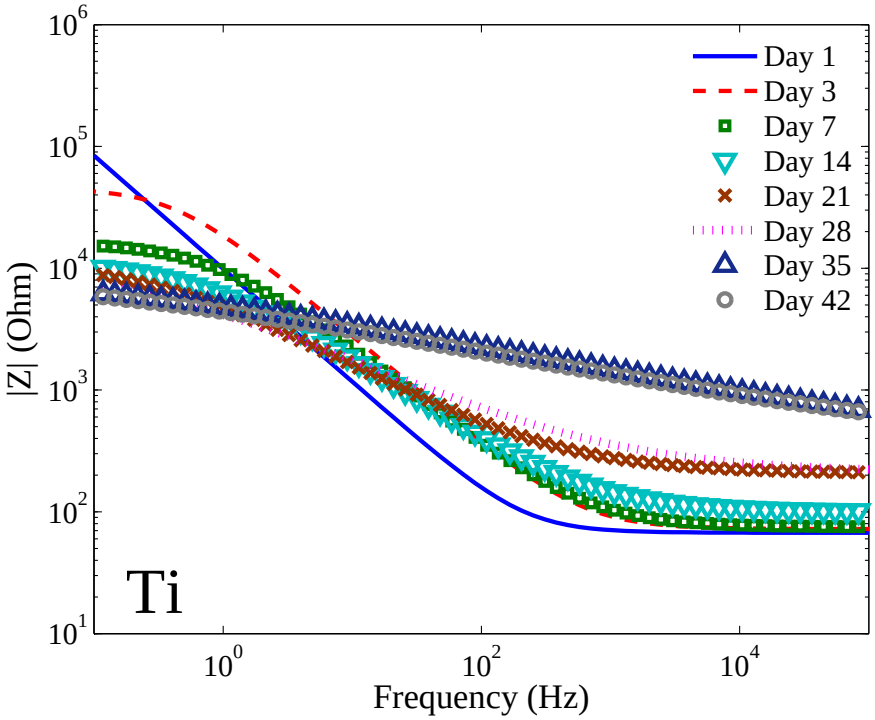

Figure 4.12: Impedance magnitude spectra of Ti electrode changing through the 42-day experimental period.

Table 4.6: Electrode/Electrolyte interface model parameters changing through 42 days of immersing Ti electrode in PBS solution obtained from fitting experimental data to model.

	Ti		
	$K(\times 10^{-5})$	β	$R_{ct}(k\Omega)$
Day 1	2.2	0.93	3600
Day 3	0.9	0.89	46
Day 7	1.6	0.81	16.5
Day 14	2	0.70	11.8
Day 21	5.2	0.60	11.7
Day 28	7	0.50	11
Day 35	8.2	0.25	10.5
Day 42	9.6	0.25	10.5

4.6 Discussion of Experimental Results

Experimental results reveal that the impedance magnitude is material dependent. The reason for this material dependence was found to be the difference in cut-off frequency and beta value of each material. Cut off frequencies shift toward lower frequencies with the increase of the double layer capacitance and decrease of the deposition pressure. This phenomenon is related to the surface morphology, structural quality and deposition parameters of the electrodes. The AFM evaluations demonstrate that Au electrodes offer the smoothest surface followed by Pt and Ti respectively. Ti films deposited under lower pressure have rougher surfaces. Higher values of surface roughness provide bigger real surface areas resulting in bigger values of double layer capacitance. Hence, as explained in Chapter 3, cut off frequency is shifted toward lower frequencies leading toward better conductivity in lower frequency range. However, compared to Ti, Pt electrodes with higher f_c are proposed for implantable stimulation electrodes due to their lower impedance which is related to their lower β values.

In terms of longevity, Au electrochemical stability for 42-day evaluations is detected as the best followed by Pt and Ti, respectively. Modeling results reveal that Au electrode kept its β value close to one, which was a testimony of its ability to perform reversible capacitive reactions even after 42 days of electrode insertion into the PBS solution.

Chapter 5

Cyclic Voltammetry Studies

In order to understand the possibility of mechanisms of tissue trauma induced by electrical stimulation, charge transfer processes that occur within a very narrow zone close to the electrode surface, at the electrode/electrolyte interface must be studied. To do so, some electrochemical methods are used. In addition to electrochemical impedance spectroscopy (EIS) that was discussed in previous chapters, cyclic voltammetry (CV) technique also reveals some quantitative information about the interfacial processes and safe limits to avoid the tissue injury. In this chapter cyclic voltammogram of each electrode is measured. It is then used to explore the charge transfer reactions and calculate the charge delivery capacity (CDC) of the electrodes. Differences are explained and electrodes are compared based on the safety limits they provide.

5.1 Cyclic Voltammograms and Charge Transfer Mechanisms

In cyclic voltammetry the voltage is swept between two values at a fixed rate, and the corresponding current that flows is monitored. As explained in Chapter 3, this data is then plotted as current density (i/A) versus potential (E), and is called cyclic voltammogram. To follow the safe electrochemical limits from the literature [4,52,53], the electrode potentials versus the Calomel reference electrode is kept within the 'water window'. The water window includes the potential range that avoids the electrolysis of water. Electrolysis of water can occur through the following reactions:

$$2H_2O \rightarrow O_2(g) + 4H^+ + 4e^- \tag{5.1}$$

$$2e^- + 2H^+ \rightarrow H_2\,(g) \tag{5.2}$$

Reaction 5.1, which is the evolution of oxygen, occurs if the working electrode is served as anode, and reaction 5.2, which is the reduction of hydrogen, takes place when working electrode is made a cathode [52]. These reactions are harmful due to the possible physical damage that the produced gas causes, since the produced gas can not be reversed by changing the direction of voltage sweep. Hence, they form the local pH change near the electrode, and thus, must be avoided. Reaction 5.1 occurs at potentials over $1.47\ V$ and reaction 5.2 occurs at potentials below $-0.6\ V$ versus saturated calomel (SCE) reference electrode. Therefore, for performing CV measurements in PBS solution, the water window of $[-0.6, 0.8]V$ is selected.

5.1.1 Pt Electrode

Figure 5.1 shows the cyclic voltammogram of Pt electrode submerged in $0.1\ M$ phosphate buffered saline (PBS) solution within the water window at a scan rate of $100\ mVs^{-1}$.

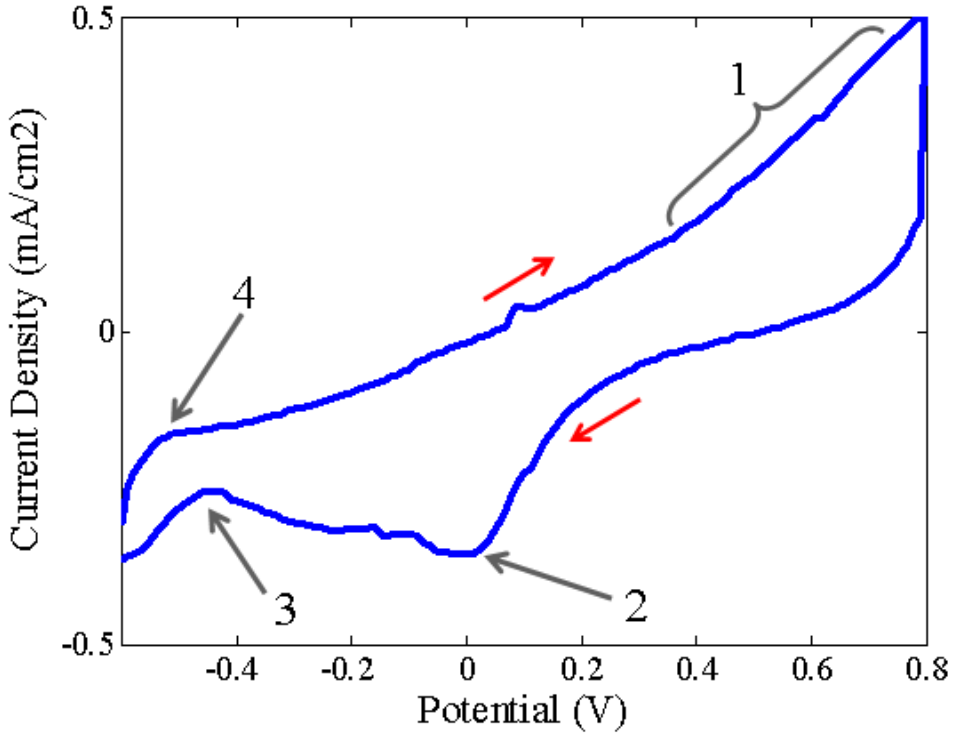

Figure 5.1: Cyclic Voltammogram of Pt Electrode in 0.1 M PBS Solution. The reactions are highlighted with numbers as,(1) Oxide formation, (2) oxide reduction, (3) hydrogen adsorption and (4) hydrogen desorption.

In this voltage range, platinum electrode faces several oxidation changes. On the positive sweep, platinum starts reacting with oxygen in water, forming platinum oxide. A small shoulder is reported to be formed at potentials shown as (1) in Figure 5.1, which is assigned to oxide formation [53]. However, such shoulder is not observed in our Pt CV curve. Each platinum atom could be bound to a maximum of 2 oxygen atoms, resulting in a $+4$ state. On the negative sweep, as the voltage falls below $0.1\ V$, the oxide is reversed to elemental

platinum. The peak at $-0.05\ V$ shown as (2) corresponds to oxide reduction. Next observed peak at more negative voltages near $-\ 0.4\ V$, (peak 3) is due to platinum's excess electrons which result in hydrogen atoms bonding to platinum. Finally peak 4 indicates hydrogen desorption. Platinum redox potentials are listed in Table 5.1 from [40, 52].

Table 5.1: Platinum reactions and redox potentials in accordance with standard hydrogen electrode [40, 52].

Reaction	$E^o\ vs.\ SCE$
$Pt + H_2O \rightleftarrows PtO + 2H + 2e^-$	$0.3\ V$
$PtO + H_2O \rightleftarrows PtO_2 + 2H^+ + 2e^-$	$0.35\ V$
$Pt - H \rightleftarrows Pt + H^+ + e^-$	$-0.4\ V$
$Pt\ (-)\ repels\ Cl^- \rightleftarrows Pt\ (+)\ attracts\ Cl^-$	

It should be noted that these reactions are reversible. If the redox couple is reversible then when the applied potential is reversed, it will reach the potential that reoxidizes the product formed in the first reduction reaction, and produce a current of reverse polarity from the forward scan. This oxidation peak will usually have a similar shape to the reduction peak. As a result, information about the redox potential and electrochemical reaction rates of the compounds are obtained.

In the case of Pt electrode, the first two equations are the oxidation and reduction of platinum electrode. The third reaction is the hydrogen atom plating process which occurs at low potentials. It minimizes possible metal dissolution, and it is kinetically reversible. The last reaction is the double layer charging/discharging process. Through this reaction, the ions are attracted and repelled from the bulk of the solution to the area close to the

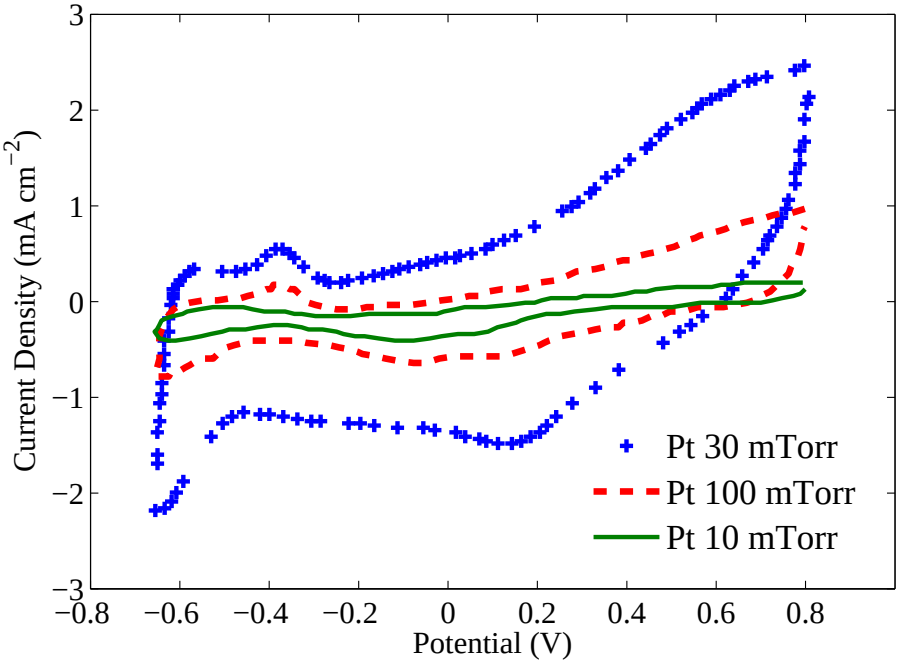

Figure 5.2: Cyclic Voltammogram of Pt Electrode deposited at different working pressures measured in 0.1 M PBS solution at a scan rate of 100 mVs^{-1} [3].

metal surface. Since no chemical change occurs, this redistribution of the ions at the electrode/electrolyte interface is reversible and safe [40, 52].

Similar to the literature [3, 20, 53], not perfectly but roughly symmetrical CV plots along the potential axis are observed for Pt. Lee *et. al* [3] performed similar cyclic voltammetry studies on Pt electrode. However, the fabrication parameters were different from our parameters. As Figure 5.2 shows, CV curve with qualitatively similar redox peaks and shoulders was obtained.

5.1.2 Au Electrode

Figure 5.3 (a) shows the cyclic voltammogram of Au electrode. For Au, unequal cathodic and anodic charge transfer occurs through the films and the electrolyte.

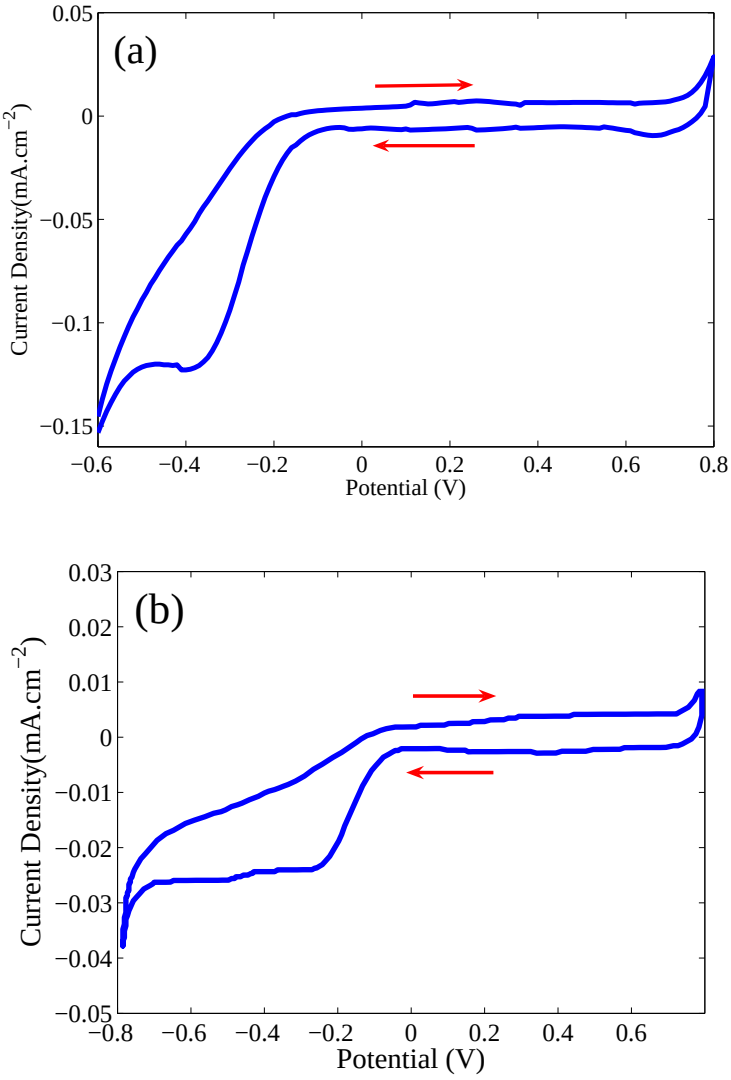

Figure 5.3: Cyclic voltammogram of Au electrode at scan rate of $100\ mVs^{-1}$ measured in (a) 0.1 M PBS solution (this study) and (b) 0.2 M PBS Solution [4].

As Figure 5.3 (a) suggests, capacitive processes are observed between -0.1 and $0.7\ V$. No faradaic electron transfer takes place in this range. However, at potentials less than $-0.2\ V$, the observed decline in current is the testimony of oxygen reduction.

This kind of behavior for gold electrode is also reported by Moulton *et. al* [4]. As shown in Figure 5.3 (b),the identical double layer behavior and oxidation peak was observed for gold measured in $0.2\ M$ PBS solution at the scan rate of $100\ mVs^{-1}$. However, they

recorded CV curves for a bigger potential sweep. At potentials below $-0.6\ V$, a sharp increase in reduction current was obtained. This sharp increase was reported to be due to the reduction of the PBS solution producing H_2 gas [4].

5.1.3 Ti Electrode

Similar to Au, Ti offers unequal cathodic and anodic charge transfer through the films and the electrolyte. For Ti, only one reversible oxidation reaction is reported within the water window [40], as Equation 5.3:

$$2TiO_2 + 2H^+ + 2e^- \rightleftarrows Ti_2O_3 + H_2O \tag{5.3}$$

However, this kind of behavior is not observed in this study as shown in Figure 5.4, at the reported reduction potential of $-0.54\ V$. As Figure 5.4 displays, for titanium, between -0.6 and $0.4\ V$, capacitive reactions are observed. Above $0.6\ V$, Ti behavior seems similar to Pt reported behavior in nitrogen-purged PBS at $1.0 - 1.5\ V$ applied voltage [53].

A possible cause could be oxidation of the chloride ion and oxidation of a phosphate group. Besides, it should be noted that for Ti deposited at the pressure of $10^{-6}\ Torr$, the higher pressure results in lower vacuuming. This increases the amount of molecules that can cause the creation of titanium oxide rather than a titanium layer. Therefore, it is possible that with the higher deposition pressure a titanium oxide film have been created rather than a titanium one. To help understand the difference in the CV response, some thin film structure and composition characterization work is suggested.

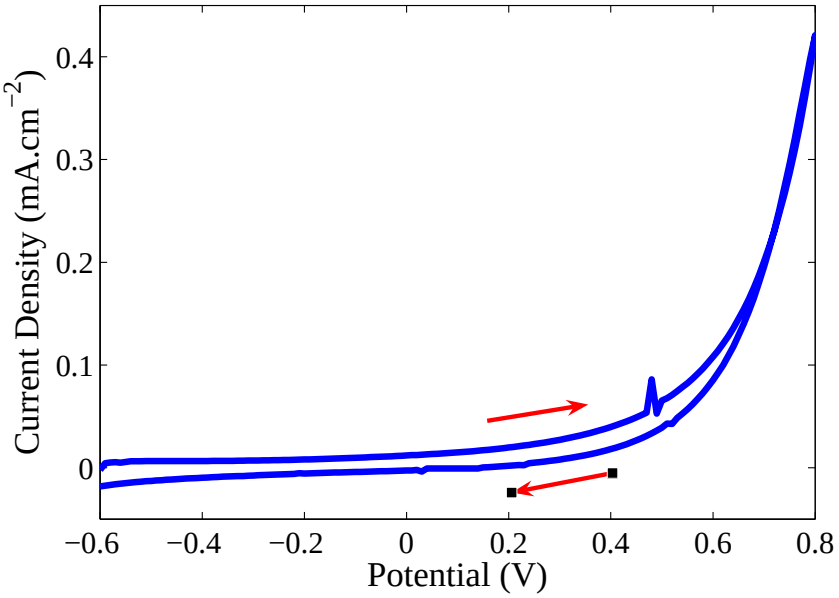

Figure 5.4: Cyclic Voltammogram of Ti Electrode in 0.1 M PBS Solution.

5.1.4 Ti Electrode Deposited at Lower Pressure

The cyclic voltammogram of Ti electrode deposited at lower deposition pressure is shown in Figure 5.5. Similar to Pt, faradaic-dominated behavior is seen for this type of Ti electrode. Further, not perfectly but roughly symmetrical CV plot along the potential axis is observed which shows the reversibility of the reactions.

5.2 Charge Delivery Capacity

Besides studying the charge transfer reactions, another application of cyclic voltammetry is to investigate the charge delivery capacity (CDC) of electrodes. As explained in Chapter 3, charge delivery capacity is the total quantity of charge that may be injected into, transferred through or stored in the electrode reversibly. This include double layer capacitance, pseudocapacitance, or any reversible faradaic processes.

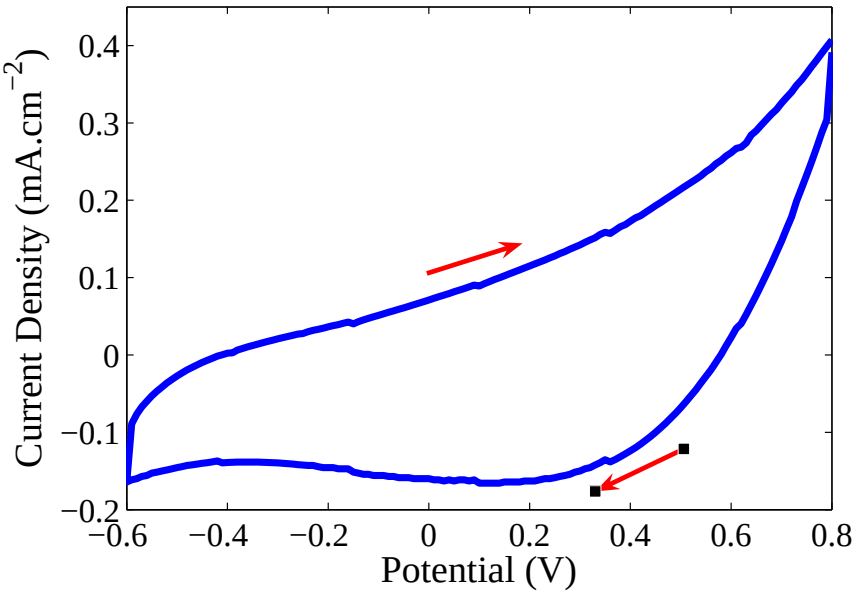

Figure 5.5: Cyclic voltammogram of Ti electrode deposited at lower pressure in 0.1 M PBS solution.

In neuromuscular electrical stimulation, high CDC electrode is demanded. A high CDC electrode can handle a relatively large amount of injected charge without causing any damage to either the tissue, which is stimulated, or the electrode itself. In addition, higher value of CDC would require smaller area to transfer certain amount of charge. Since practical applications require miniaturized electrode geometry to control a large number of different muscles, high charge delivery capacity material is demanded [13, 25, 26, 35].

This CDC value is calculated from the CV curves by integrating the current with respect to voltage, over the voltage sweep range of $-0.6\ V$ to $0.8\ V$ in reference to Equation 3.3. In other words, the area obtained inside the CV curve represents the value of charge delivery capacity.

In order to compare the CDC values qualitatively, Figure 5.6 represents the cyclic voltammograms of Pt, Ti, Au, and Ti deposited at lower base pressure. Calculated CDC values of high pressure deposited electrodes at $1 \times 10^{-6}\ \ Torr$ are shown in Table 5.2 in

comparison with their values from the literature. According to Figure 5.6 and Table 5.2, Pt electrode with largest enclosed area shows the highest CDC followed by Au and Ti.

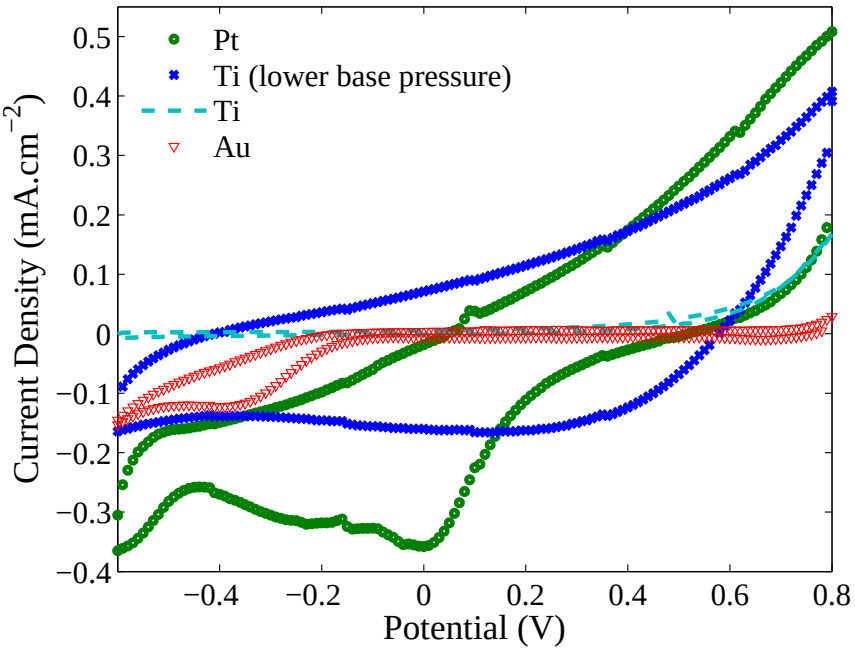

Figure 5.6: Cyclic voltammogram of Ti electrode deposited at lower pressure in 0.1 M PBS solution.

However, as deposition pressure decreases to $3 \times 10^{-8}\ Torr$, Ti CDC value increases to $2.91\ mC\ cm^{-2}$. The increase in the CDC observed at the lower deposition pressure is likely related to structural and/or compositional changes in the deposited film, which are known to be dependant on deposition conditions [54]. The controlling factors at play require further study. S. Negi *et. al* [20] and S. Lee *et. al* [3] reported the identical increase of CDC in the Pt, Ir and IrO_2 with the decrease of radio-frequency sputtering pressure. The sputtering pressure was decreased from 100 to 5, and from 100 to $30\ mTorr$, respectively.

Table 5.2: Calculated CDC values from CV curves of high pressure deposited electrodes in this study compared to their values from literature.

	CDC Value $(mC\ cm^{-2})$	
Films	**This Study**	**Literature**
Pt	3.12	2.92-26.8 [3], 4.4 [55]
Au	0.33	0.24 [56]
Ti	0.20	0.59 [56]

5.3 Discussion of Experimental Results

Experimental results show the significance of cyclic voltammetry measurements in addition to electrochemical impedance spectroscopy. Through CV tests, the electrochemical processes of each electrode while immersed in PBS solution was elucidated. Reversibility of reactions and the stimulation limits were determined.

Charge delivery capacities of Pt, Ti and Au were calculated from CV graphs to evaluate the electrodes capability of performing reversible charge transfer. It was found that Pt electrodes offer the best CDC value followed by Au and Ti ones. In the case of deposition pressure, it was shown that lower deposition pressure provides higher charge delivery capacity.

Chapter 6

Discussion and Perspective

According to the interfacial impedance studies in Chapter 4, electrochemical conductivity of electrode at the electrolyte depends on several factors including the electrodes size, material and the deposition pressure. The interface modeling results reveal that the dependence of impedance magnitude is due to the cut off frequency and capacitive quality (β) of the electrode/electrolyte interface that each size, material or deposition condition presents. As shown in Figures 4.3 and 4.7 and T able 4.2, cut off frequencies shift toward lower frequencies with the increase of the double layer capacitance. Further, decrease in deposition pressure of Ti electrode has also the similar effect on its cut off frequency. This phenomenon is based on the surface characteristics, structural quality and deposition conditions of the electrodes. The AFM evaluations demonstrate that Au electrodes suggest the smoothest surface followed by Pt and Ti, respectively. Ti films deposited under lower pressure offer higher values of surface roughness. Rougher surfaces provide larger real surface area resulting in increased double layer capacitance. Hence, cut off frequency is shifted toward lower frequencies leading toward better conductivity in lower frequency range. However, compared to Ti, Pt electrodes with higher f_c are proposed for implantable

stimulation electrodes due to their lower impedance that is related to lower β values.

In terms of longevity, modeling results reveal that Au electrode tends to sustain its capacitive quality (β value) to perform reversible capacitive reactions even after 42 days of electrode insertion into the PBS solution, followed by Pt and Ti electrodes, respectively.

Based upon the cyclic voltammetry measurements presented in chapter 5, it is inferred that Pt electrode offers the highest charge delivery capacity (CDC) value followed by Au and Ti. In the case of deposition pressure, it was shown that lower deposition pressure provided Ti electrodes with higher charge delivery capacity.

All in all, these results may make lower pressure deposited Pt electrode with high conductivity and CDC the best material for the short term applications of neuromuscular electrical stimulation. Whereas, Au electrode possessing improved stability but lower conductivity and CDC is suggested for long term applications.

However, it should be noted that all these results are based on the electrochemical perspective which does not consider some physiological concerns. These concerns include the core body temperature and the excitation frequency. All the experiments presented in this research were performed at room temperature. In practical applications, however, the implanted electrodes work at the body core temperature that is $37\ ^{o}C$. At this temperature the impedance magnitude changes. CV curves would also differ as the standard potential values of the interfacial reactions are temperature-dependent.

In addition, as discussed in Chapter 5, due to the limitation of equipment, the fastest possible measurement was performed at the scan rate of $100\ mV.s^{-1}$, which imitates stimulation at a frequency of $0.072\ Hz$. This sweep is much slower compared to the frequency range of NMES. For instance, pacemakers need to be able to function at frequencies as

high as $10\ KHz$. Therefore, to study the electrochemical properties of deposited electrodes at conditions more similar to practical applications, some faster CV measurements are required.

The perspective application for the implantable and flexible stimulation electrode is the neuromuscular prosthetic system as presented in Figure 6.1.

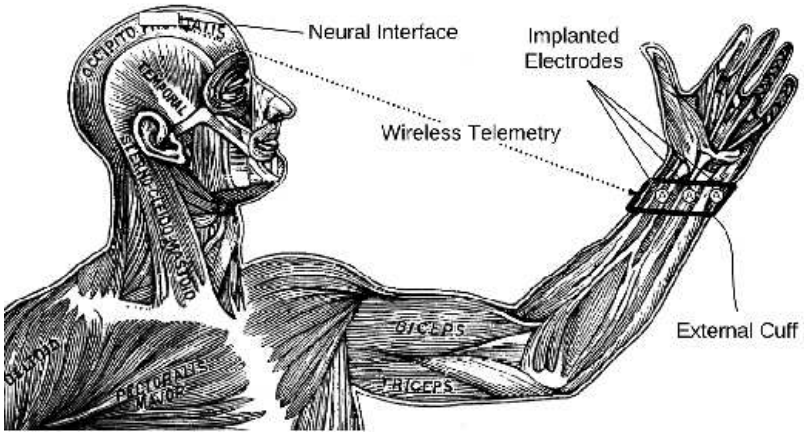

Figure 6.1: Schematic of a neuromuscular prosthetic system [57] (with permission of Dr. T. E. Doyle. Original line art courtesy of FCIT.)

Neuromuscular prostheses have drawn much attention with their success in restoring functional movement to paralyzed limbs [6, 58, 59]. By stimulating the nerves that activate the muscular contraction, less activation current is required than electrically activating the muscle directly. To restore a motor behavior, such as grasping an object, up to eight muscles should be activated and controlled. Yet, miniaturized electrode geometry is required in improved devices to control this large number of different muscle fascicles selectively and independently with causing no tissue injury. This demands that fabricated electrodes provide enhanced stability and charge transfer parameters, such as increased charge delivery capacity and electrode/tissue conductivity in the desired frequency range of stimulation.

One of the proposed NMES prosthetic systems is called BION, which was first introduced by Loeb et al. *et al.* [7] as an injectable microstimulator. BION system consists of four main parts [5]; (1) the BION stimulator, which includes an implantable pulse generator, stimulating electrodes, battery and an antenna for wireless telemetry as shown in Figure 6.2, (2) a recharging system for its battery, (3) a remote control and (4) a clinician's programmer. The clinician's programmer is a software installed on a computer. This software allows the clinician to set the stimulation parameters of the BION (such as frequency, stimulation waveform and its amplitude range). The user can then use the remote control to control the transmission of adjusted power and command signals during his daily activities. The remote control has an inductive coil that should be worn over or placed close to the implants and uses a wireless telemetry system to transmit power and command signals. Implanted BION receives power and digital command signals from the remote control through its antenna. As the implant detects a match to its address, an excitation impulse is generated and stimulation electrodes transfer the impulse to the desired nerves resulting in muscle contraction.

Therefore, BION device uses the address matching to derive the signals to electrodes. However, there is a challenge for signals to be derived to the electrodes. The challenge rises as the electrodes may be in contact with many nerves that control different muscle fibers providing various functions. In order to address the correct activation, a microprocessor is designed in some NMES prostheses, as shown in Figure 6.3, to control the transmission of the derived signals to the stimulating electrodes [60]. This microprocessor detects that received stimulus should be delivered to which nerve as the patient decides to move a prosthetic limb. It should be noted that there are some other approaches to control the stimulating electrodes. These approaches include electronic and mechanical switches which

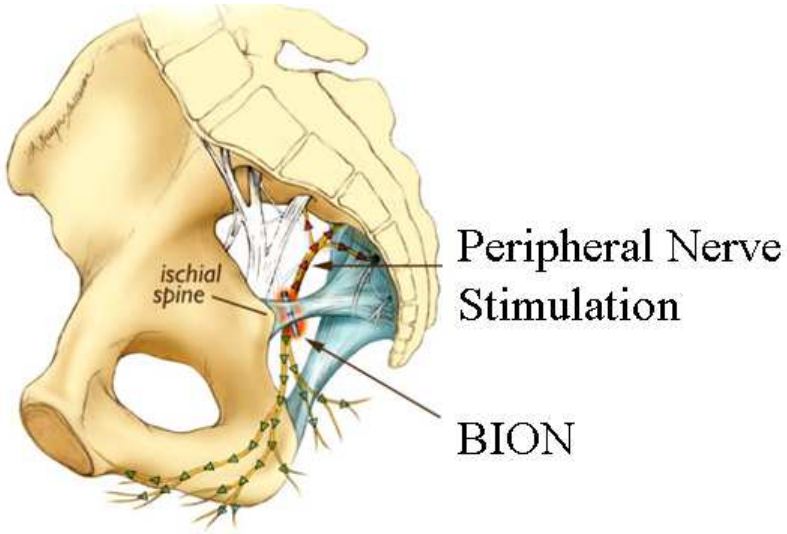

Figure 6.2: Schematic of a placed BION implant for peripheral nerve stimulation (pudendal nerve) [5]. The stimulating electrodes are placed on the outside of the BION. Note that the triangles show the propagation of impulses through peripheral nerves

are activated by the user [6]. Current standard NMES prostheses only control a limited number of patterns such as 1 or 2 joints (elbow flexion/extension). However, the implanted electrodes should be able to transfer pulses of 2 to 512 μS in $2 - \mu S$ steps. BION has the capability to receive up to 3000 commands per second resulting in a selective activation of muscle fascicles [5, 60]. Therefore, implantable electrodes require to satisfy these harsh working conditions and thus, should be electrochemically investigated.

With the presented electrode properties, the author believes deeper insight has been yielded to the primary challenges of interface impedance, stability and charge transfer to the biological system through flexible LCP substrate with deposited electrode materials for a wide range of stimulation frequencies.

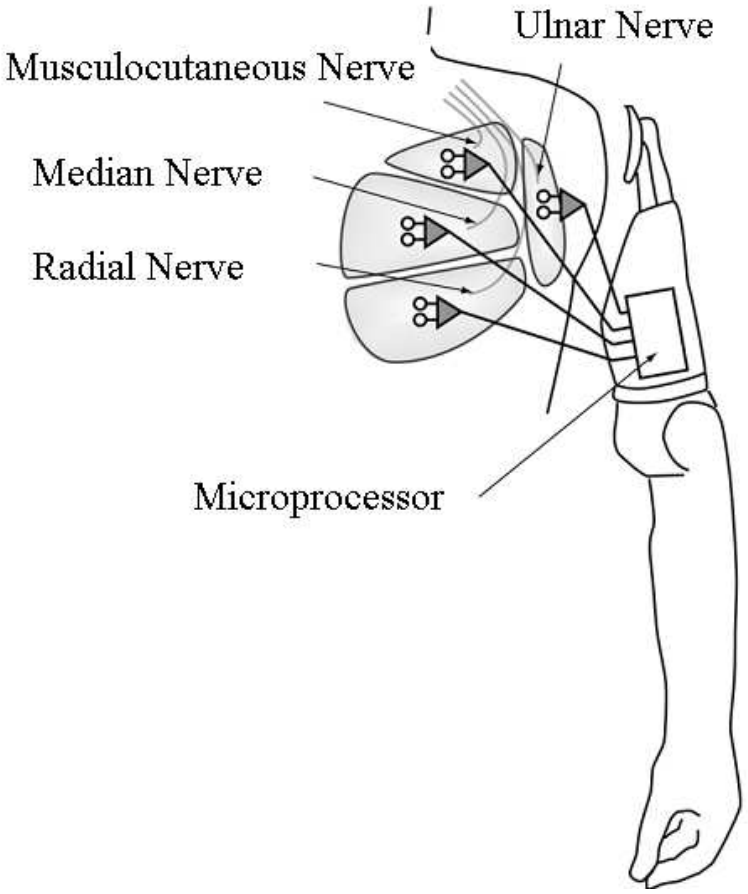

Figure 6.3: Schematic of targeted muscle reinnervation of peripheral nerves. It shows that a microprocessor can provide a selective activation [6]

.

Chapter 7

Conclusions and Future Works

7.1 Conclusions

This research studies the electrochemical reactions and parameters of Platinum (Pt), Gold (Au), and Titanium (Ti) deposited on liquid crystal polymer (LCP) to understand the charge transfer mechanisms of implantable electrodes for neuromuscular electrical stimulation.

Electrodes were fabricated through e-beam evaporation and characterized using atomic force microscopy (AFM), electrochemical impedance spectroscopy (EIS) and cyclic voltammetry (CV) measurements. A theoretical model was proposed to explain physical functionalities and assess the electrodes performance.

The results show that as the size of electrode increases, higher conductivity and higher double layer capacitance are obtained. In neuromuscular stimulation frequencies of 1-250 Hz, Pt electrodes offer the highest relative conductivity followed by Ti and Au respectively. In higher frequencies (frequencies above their f_c), similar impedance magnitudes are observed. This material dependence of impedance magnitude is due to the surface

morphology, structural quality and deposition parameters of the electrode. According to AFM data, Au electrodes offer the smoothest surface followed by Pt and Ti respectively. Higher values of surface roughness provide bigger real surface areas resulting in bigger magnitudes of double layer capacitance. Hence, better conductivity is obtained in lower frequency range.

In terms of longevity, Au electrochemical stability through the 42-day evaluations is detected as the best followed by Pt and Ti, respectively. Modeling results reveal that Au electrode keeps its capacitive quality (β value) to perform reversible capacitive reactions even after 42 days of electrode insertion into the PBS solution.

Charge delivery capacities of Pt, Au and Ti were calculated from CV graphs to elucidate the electrodes capability of performing reversible charge transfer. It is found that Pt offers the best CDC value followed by Au and Ti. In the case of deposition pressure, it is shown that for Ti electrode lower deposition pressure provides higher charge delivery capacity.

In Conclusion, lower pressure deposited Pt electrode with high conductivity and CDC may make the best material for the short term applications of neuromuscular electrical stimulation. Whereas, Au electrode possessing improved stability but lower conductivity and CDC is suggested for long term applications This result could help in better design and miniaturization of electrochemical electrodes for the further development of neuromuscular prostheses.

7.2 Future Works

The future work could be directed to the followings:

- Investigation on the causes of the drops in charge transfer resistance (R_{ct}) and capacitive quality (β) of the electrode/electrolyte interface with elapsing time.

- Fabrication of other thin film electrodes (rather than titanium) in lower deposition pressure, and comparatively studying the electrochemical interfacial charge transfer parameters. The engaged factors for the increase in the CDC value observed at the lower deposition pressure could be due to structural and/or compositional changes in the deposited films, which are known to be dependant on deposition conditions and require further study to be determined. Besides, long-term stability of low pressure deposited electrodes could be compared to the high pressure ones. Elucidating the effect of deposition pressure on all electrode types responses, definite conclusions could be derived.

- Performing some thin film structure and composition characterization work to help understand the differences in the CV response of high pressure deposited titanium electrodes in different studies.

- Fabrication of micro/nano meter size electrodes that can be realized through surface activated nanobonding of metals on liquid crystal polymer, as it provides strong adhesion for any kind of thin material on polymer [61–64].

- Conducting cyclic voltammetry measurements for several activation cycles and observing the changes to get better insights of the processing electrochemical reactions during electrical stimulation.

- Micro-electro-mechanical systems and nanotechnology could be applied to form nano array electrodes on liquid crystal polymer to yield more efficient neuromuscular activation [65].

- One of the future focuses could be to address faster sweeps of CV and CV/EIS measurements without a reference electrode (since practical excitation is performed with only anode and cathode without any reference electrode) and at higher temperature (close to body core temperature of 37^oC) could provide more realistic results as the conditions are more similar to those of practical applications. However, such measurements exceed the limitations of current equipment.

Bibliography

[1] E. McAdams, J. Jossinet, R. Subramanian, and R. McCauley, "Characterization of gold electrodes in phosphate buffered saline solution by impedance and noise measurements for biological applications," in *28th Annual International IEEE Conference of Engineering in Medicine and Biology Society (EMBS)*, pp. 4594 –4597, Sept. 2006.

[2] N. Tandon, C. Cannizzaro, E. Figallo, J. Voldman, and G. Vunjak-Novakovic, "Characterization of electrical stimulation electrodes for cardiac tissue engineering," in *28th Annual International IEEE Conference of Engineering in Medicine and Biology Society (EMBS)*, pp. 845 –848, Sept. 2006.

[3] S. H. Lee, J. H. Jung, Y. M. Chae, J. F. Suh, and J. Y. Kang, "Fabrication and characterization of implantable and flexible nerve cuff electrodes with pt, ir and irox films deposited by rf sputtering," *Micromechanical and Microengineering*, vol. 20, no. 3, pp. 035015–035023, 2010.

[4] S. Moulton, J. N. Barisci, A. Bath, R. Stella, and G. G. Wallace, "Studies of double layer capacitance and electron transfer at a gold electrode exposed to protein solutions," *Electrochemica Acta*, vol. 49, no. 24, pp. 4223–4230, 2004.

[5] R. Carbunaru, T. Whitehurst, K. Jaax, J. Koff, and J. Makous, "Rechargeable battery-powered bion reg; microstimulators for neuromudulation," in *26th Annual International Conference of the IEEE on Engineering in Medicine and Biology Society*, vol. 2, Sept. 2004.

[6] A. E. Schultz and T. A. Kuiken, "Neural interfaces for control of upper limb prostheses: The state of the art and future possibilities.," *Physical Medicine and Rehabilitation*, vol. 3, no. 1, pp. 55–67, 2011.

[7] G. Loeb and C. J. Zamin, "Injectable microstimulator for functional electrical stimulation," *Transducers and Electrodes*, vol. 29, pp. NS13–NS19, 1991.

[8] S. F. Cogan, "Neural stimulation and recording electrodes," *Annual Review of Biomedical Engineering*, vol. 10, no. 1, pp. 275–309, 2008.

[9] W. M. Grill, "Electrical stimulation for control of bladder function," in *31st IEEE Conference on Engineering in Medicine and Biology Society (EMBS)*, pp. 2369–2370, Sept. 2009.

[10] D. K. Peterson, M. L. Nochomovitz, T. A. Stellato, and J. T. Mortimer, "Long-term intramuscular electrical activation of the phrenic nerve: Efficacy as a ventilatory prosthesis," *IEEE Transaction on Biomedical Engineering*, vol. 41, pp. 1127–1135, Dec. 1994.

[11] J. D.Weiland, W. Liu, and M. S. Humayun, "Retinal prosthesis," *Annual Review of Biomedical Engineering*, vol. 7, pp. 361–401, 2005.

[12] F. Zeng, S. Rebscher, W. Harrison, X. Sun, and H. Feng, "Cochlear implants: System design, integration, and evaluation," *IEEE Reviews on Biomedical Engineering*, vol. 1, pp. 115–142, 2008.

[13] J. D. Weiland, D. J. Anderson, and M. S. Humayun, "In vitro electrical properties for iridium oxide versus titanium nitride stimulating electrodes," *IEEE Transactions on Biomedical Engineering*, vol. 49, pp. 1574–1579, Dec. 2002.

[14] K. Singh, F. J. R. Richmond, and G. E. Loeb, "Recruitment properties of intramuscular and nerve-trunk stimulating electrodes," *IEEE Transactions on Rehabilitation Engineering*, vol. 8, pp. 276 –285, Sept. 2000.

[15] Y. Shacham-Diamond, S. Krylov, T. Shmilovich, R. O. Almog, N. Fishelson, Y. Sverdlov, I. Torchinsky, G. Rosenman, A. Inberg, and O. Berkh, "Metallization technologies and strategies for plastic based biochips, sensors and actuators for healthcare and medical applications," *ECS Transaction*, vol. 23, no. 1, pp. 243–254, 2009.

[16] F. J. Rodriguez, D. Ceballos, M. Schuttler, A. Valero, E. Valderrama, T. Stieglitz, and X. Navarro, "Polyimide cuff electrodes for peripheral nerve stimulation," *Neuroscience Methods*, vol. 98, pp. 105–118, 2000.

[17] K. Takata and A. Pham, "Electrical properties and practical applications of liquid crystal polymer flex," in *6th IEEE Conf. on Polymers and Adhesives in Microelectronics and Photonics*, Oct. 2007.

[18] N. R. Armstrong and R. K. Quinn, "Auger and x-ray photoelectron spectroscopic and electrochemical characterization of titanium thin film electrodes," *Surface Science*, vol. 67, pp. 451–468, 1977.

[19] A. Ouerd, C. Alemany-Dumont, G. Berthome, B. Normand, and S. Szunerits, "Reactivity of titanium in physiological medium," *Journal of The Electrochemical Society*, vol. 154, no. 10, pp. C593–C601, 2007.

[20] S. Negi, R. Bhandari, L. Rieth, and F. Solzbacher, "Effect of sputtering pressure on pulsed-dc sputtered iridium oxide films," *Sensors and Actuators B: Chemical*, vol. 137, no. 1, pp. 370 – 378, 2009.

[21] L. L. Baker, J. Chae, and L. R. S. et al, *Neuromuscular Electrical Stimulation: A Practical Guide*. Los Amigos Research and Education Institute, Inc., 2008.

[22] W. Faloon, R. L. Waters, D. R. McNeal, and B. Clikord, "Functional electrical stimulation of the peripheral nerve for hemiplegia. long-term clinical follow-up," *Journal of Bone and Joint Surgery*, vol. 67, pp. 792–793, 1985.

[23] A. Kuhn and T. Keller, "Electrodes for transcutaneous (surface) electrical stimulation," *Journal of Automatic Control*, vol. 18, no. 2, pp. 35–45, 2008.

[24] C. L. Lynch and M. R. Popovic, "Functional electrical stimulation," *IEEE Control Systems Magazine*, vol. 28, no. 2, pp. 40–50, 2008.

[25] B. D. Ratner, *Biomaterials Science*. Elsevier Academic Press, 2nd edition, 2004.

[26] D. R. Merrill, *Implantable Neural Prostheses 2, Biological And Medical Physics Biomedical Engineering*. Springer New York, 2010.

[27] J. H. M. Put, W. L. C. Rutten, and H. J. van Wier, "Sensitivity and selectivity of intraneural stimulation using a silicon electrode array," *IEEE Tranaction on Biomedical Engineering*, vol. 38, no. 2, pp. 192–198, 1991.

[28] D. R. Kipke, K. J. Otto, and M. D. Johnson, "Voltage pulses change neural interface properties and improve unit recordings with chronically implanted microelectrodes," *IEEE Tranaction on Biomedical Engineering*, vol. 53, no. 2, pp. 333–340, 2006.

[29] L. Rieth, M. Topper, R. A. Normann, F. Solzbacher, R. Bhandari, and S. Negi, "Wafer level processing of silicon arrays for implantable medical devices," in *Electronic Components and Technology Conference*, pp. 1567–1572, Jun. 2007.

[30] K. Moxon, S. Leiser, G. Gerhardt, K. Barbee, , and J. Chapin, "Ceramic-based multisite electrode arrays for chronic single-neuron recording," *IEEE Tranaction on Biomedical Engineering*, vol. 51, no. 4, pp. 647–656, 2004.

[31] M. Schuettler, J. Meyer, T. Stieglitz, and H. Beutel, "Micromachined polyimide-based devices for exible neural interfaces," *Biomedical Microdevices*, vol. 2, no. 4, pp. 283–294, 2000.

[32] R. J. Vetter, R. Miriani, D. R. Kipke, D. S. Pellinen, and T. Moon, "Multifunctional fexible parylene-based intracortical microelectrodes," Sept. 2005.

[33] H. Tanilac, K. Djupsund, C. K. Cheunga, and P. Renaudb, "Flexible polyimide microelectrode array for in vivo recordings and current source density analysis," *Biosensors and Bioelectronics*, vol. 22, pp. 283–294, 2007.

[34] F. Keohan, X. F. Wei, A. Wongsarnpigoon, E. Lazaro, J. E. Darga, and W. M. Grill, "Fabrication and evaluation of conductive elastomer electrodes for neural stimulation," *Journal of Biomaterials Science, Polymer Edition*, vol. 18, no. 8, pp. 1057–1073, 2007.

[35] I. S. Lee, C. N. Whang, J. C. Park, D. H. Lee, and W. S. Seo, "Biocompatibility and charge injection property of iridium film fomed by ion beam assisted deposition," *Biomaterials*, vol. 24, pp. 2225–2231, 2003.

[36] K. Wang, H. A. Fishman, H. Dai, and J. S. Harris, "Neural stimulation with a carbon nanotube microelectrode array," *Nano Letters*, vol. 6, no. 9, pp. 2043–2048, 2006.

[37] Y. Lu, T. Li, X. Zhao, M. Li, Y. Cao, H. Yang, and Y. Y. Duan, "Electrodeposited polypyrrole/carbon nanotubes composite films electrodes for neural interfaces," *Biomaterials*, vol. 31, no. 19, pp. 5169 – 5181, 2010.

[38] D. C. Martin and M. R. Abidian, "Experimental and theoretical characterization of implantable neural microelectrodes modified with conducting polymer nanotubes," *Biomaterials*, vol. 29, no. 9, pp. 1273–1283, 2008.

[39] D. B. McCreery and W. F. Agnew, "Considerations for safety with chronically implanted nerve electrodes," *Epilepsia*, vol. 31, pp. S27–S32, 1990.

[40] A. Hung, I. B. Goldberg, and J. W. Judy, "Stimulation electrode materials and electrochemical testing methods," *Implantable Neural Prostheses 2*, pp. 191–216, 2010.

[41] Z. Xinghua, Y. Dingyu, W. Zhaorong, S. Hui, W. Zhiguo, and Z. Xiaotao, "Photoconductive properties of lead iodide films prepared by electron beam evaporation," *Journal of Semiconductors*, vol. 31, no. 8, pp. 083002–1–083002–4, 2010.

[42] *Scanning Probe Microscopy Training Notebook*. Veeco, 2010.

[43] C. M. A. Brett, "Electrochemical impedance spectroscopy for characterization of electrochemical sensors and biosensors," *ECS Transaction*, vol. 13, no. 13, pp. 67–80, 2008.

[44] A. Lasia, "Electrochemical impedance spectroscopy and its applications," *Modern Aspects of Electrochemistry*, vol. 32, pp. 143–248, 1999.

[45] W. Franks, I. Schenker, P. Schmutz, and A. Hierlemann, "Impedance characterization and modeling of electrodes for biomedical applications," *IEEE Transaction on Biomedical Emgineering*, vol. 52, pp. 1295–1302, July 2005.

[46] www.porous 35.com, "Electrochemical cells and potentiostats, chapter2: Electrochemical cells and potentiostats,"

[47] W. Plieth, *Electrochemistry for Materials Science*. Elsevier, 2007.

[48] *Detailed Specifications of Gamry Potentiostat*. Gamry Instruments, 2009.

[49] J. Riistama and J. Lekkala, "Electrode-electrolyte interface properties in implantation conditions," in *28st IEEE Conference on Engineering in Medicine and Biology Society (EMBS)*, pp. 6021–6024, Sept. 2006.

[50] A. Lasia, *Modern Aspects of Electrochemistry*, vol. 32. Kluwer Academic/Plenum, 1994.

[51] K.-P. Hoffmann, R. Ruff, and W. Poppendieck, "Long-term characterization of electrode materials for surface electrodes in biopotential recording," in *28th Annual International IEEE Conference of Engineering in Medicine and Biology Society (EMBS)*, pp. 2239–2242, Sept. 2006.

[52] S. B. Brummer and M. J. Turner, "Electrochemical considerations for safe electrical stimulation of the nervous system with platinum electrodes," *IEEE Transactions on Biomedical Engineering*, vol. BME-24, pp. 59–63, Jan. 1977.

[53] E. M. Hudak, J. T. Mortimer, and H. B. Martin, "Platinum for neural stimulation: Voltammetry considerations," *Journal of Neural Engineering*, vol. 7, no. 2, pp. 026005–026012, 2010.

[54] K. Cai, M. Muller, J. Bossert, A. Rechtenbach, and K. D. Jandt, "Surface structure and composition of flat titanium thin films as a function of film thickness and evaporation rate," *Applied Surface Science*, vol. 250, no. 2, pp. 252–267, 2005.

[55] S. Negi, R. Bhandari, L. Rieth, and F. Solzbacher, "In vitro comparison of sputtered iridium oxide and platinum-coated neural implantable microelectrode arrays," *Biomedical Materials*, vol. 5, pp. 015007–015016, 2010.

[56] O. Niina, T. Hirotaka, K. Yoshiuki, K. Toshiya, K. Risato, T. Tetsu, and H. Jari, "Comparison of electrode materials for the use of retinal prosthesis," *Bio-Medical Materials and Engineering*, vol. 21, pp. 83–97, 2011.

[57] S. Mohtashami, M. R. Howlader, and T. E. Doyle, "Comparative electrochemical investigation of pt, au and ti electrodes on liquid crystal polymer for the application of neuromuscular prostheses," *ECS Transaction*, 2011.

[58] J. Wolpaw, "Brain-computer interface research comes of age: Traditional assumptions meet emerging realities," *Motor Behavior*, vol. 42, no. 6, pp. 351–355, 2010.

[59] P. Brunner, L. Bianchi, C. Guger, F. Cincotti, and G. Schalk, "Current trends in hardware and software for braincomputer interfaces (bcis)," *Journal of Neural Engineering*, vol. 8, no. 2, pp. 025001–025008, 2011.

[60] K. A. Stubblefield, L. A. Miller, R. D. Lipschutz, and T. A. Kuiken, "Occupational therapy protocol for amputees with targeted muscle reinnervation," *Journal of Rehabilitation Research and Development*, vol. 46, no. 4, pp. 481–488, 2009.

[61] M. M. R. Howlader, P. R. Selvaganapathy, M. J. Deen, and T. Suga, "Nanobonding technology toward electronic, fluidic, and photonic systems integration," *IEEE Journal Of Selected Topics in Quantum Electronics*, vol. 17, no. 3, pp. 689–703, 2011.

[62] M. M. R. Howlader, M. Iwashita, K. Nanbu, K. Saijo, and T. Suga, "Enhanced cu/lcp adhesion by pre-sputter cleaning prior to cu deposition," *IEEE Transactions on Advanced Packaging*, vol. 28, p. 495502, Aug. 2005.

[63] K. Nanbu, S. Ozawa, K. Yoshida, K. Saijo, and T. Suga, "Low temperature bonded cu/lcp materials for fpcs and their characteristics," *IEEE Transactions on Components and Packaging Technology*, vol. 28, pp. 760–764, Dec. 2005.

[64] M. M. R. Howlader, T. Suga, A. Takahashi, K. Saijo, S. Ozawa, and K. Nanbu, "Surface activated bonding of lcp/cu for electronic packaging," *Material Sciemce*, vol. 40, no. 12, pp. 3177–3184, 2005.

[65] T.-L. Ren, B. Yan, J.-H. Lin, X.-M. Wu, L.-G. Wang, Y. Yang, and L.-T. Liu, "A mems-based flexible electrode array using composite substrate," in *28th Annual International IEEE Conference of Electron Devices and Solid- State Circuits (EDSSC),Hong Kong, China*, Dec. 2010.